

Chapter 6

Case Studies

This chapter explores some illustrative applications in the context of digital communications. The second-order estimation theory in the preceding chapters is developed for these selected case studies. In most examples, the focus is on closed-loop second-order schemes assuming that the small-error approximation is satisfied. The Gaussian ML estimator and the rest of ML-based approximations are numerically compared to the optimal second-order small-error solution in Chapter 4. Likewise, the related lower bounds in the presence of nuisance parameters are included for completeness (Section 2.6.1).

In the first section, some contributions in the field of non-data-aided synchronization are presented. Specifically, Section 6.1 proposes the global optimization of second-order closed-loop synchronizers and the design of open-loop timing synchronizers in the frequency domain. In Section 6.2, the problem of second-order carrier phase synchronization is addressed in case of noncircular transmissions. In this section, the ML estimator is shown to be quadratic at low SNR for MSK-type modulations. Moreover, second-order self-noise free estimates are achieved at high SNR exploiting the non-Gaussian structure of the digital modulation. In Section 6.3, the problem of time-of-arrival estimation in wireless communications is studied. The frequency-selective multipath is shown to increase the number of nuisance parameters and the Gaussian assumption is shown to apply in this case study.

In Section 6.4, the classical problem of blind channel identification is dealt with. The channel amplitude is shown to be not identifiable unless the transmitted symbols belong to a constant-modulus constellation and this information is exploited by the estimator. Finally, the problem of angle-of-arrival estimation in the context of cellular communications is addressed in Section 6.5. The Gaussian assumption is clearly outperformed for practical SNRs in case of constant-modulus nuisance parameters and closely spaced sources. In this section, the importance of the multiple access interference (MAI) is emphasized and MAI-resistant second-order DOA trackers are derived and evaluated.

6.1 Non-Data-Aided Synchronization

The problem of blind frequency estimation was adopted in the core of the dissertation –Chapters 3 and 4– to illustrate the most significant conclusions of this thesis. This choice was based on the relevance of this problem in many applications and, the existence of closed-form expressions for the feedforward frequency estimator considered in Chapter 3. In this section, some additional contributions in the field of non-data-aided (NDA) digital synchronization are presented and simulated.

To introduce the reader to the problem of digital synchronization, a brief review of the state-of-the-art is provided in Section 6.1.1, in which the most successful timing and frequency estimators are presented. Afterwards, in Section 6.1.2, the signal model for digital synchronization is reviewed and some important remarks are made on the structure of the transfer matrix $\mathbf{A}(\boldsymbol{\theta})$. Based on this signal model, the performance of the most important NDA (quadratic) timing estimators –for both linear and CPM modulations– is extensively evaluated via simulation in Section 6.1.5. In this context, a closed-form expression for the optimal second-order *open-loop timing* estimator is deduced by processing the received signal in the frequency domain (Section 6.1.3). Another contribution of this section is the *global* optimization of closed-loop estimators, showing that the discriminator should be designed to minimize the variance of the low-pass noisy terms because the high-pass terms (e.g., the self-noise) are filtered at the loop-filter (Section 6.1.4). Finally, all these results are validated via simulation in Section 6.1.5.

6.1.1 Overview

In digital communications, the receiver has to recover some reference parameters in order to demodulate the received signal. These parameters are mostly the signal timing and, in band-pass coherent communications, the carrier phase and the carrier frequency. The knowledge of these parameters is necessary to synchronize the demodulator and take reliable decisions on the transmitted symbols [Men97][Vaz00].

Despite the data symbols are a priori unknown, digital modulations exhibit a strict-sense *cyclostationarity* that can be exploited to derive sufficient statistics for the estimation of the aforementioned parameters. Thus, all the methods in the literature for non-data-aided (NDA) timing and frequency estimation make use of the cyclostationarity property of the received signal [Rib94].

As trying to exploit the entire statistics would be unpractical, two main directions have been adopted in the development of practical algorithms. The first direction focuses on an explicit exploitation of the second-order cyclostationarity [Gar86b][Rib94]. As a result, the algorithms derived become quadratic with respect to the received signal. There are, at least, two motivations

for choosing the second-order statistics. The first one is that it represents a minimum complexity constraint. The other is that it allows extracting useful insights from the spectral correlation concept [Gar86b], which is useful for guiding the designer in the derivation of synchronization algorithms. Although all the above methods start from a solid theoretical foundation, the second order constraint appears as an ad hoc selection, and the obtained methods are based on heuristic reasoning. For the preliminary issues on cyclostationarity the reader is referred to [Gar94] and references therein.

The second direction commonly adopted for the design of synchronization algorithms is the application of the well-known maximum likelihood principle explained in Section 2.3 [Men97][Vaz00]. While the cyclostationary framework is useful for the derivation of both feed-forward and feedback structures, the ML criterion leads *primarily* to feedback schemes (Section 2.5). With the purpose of deriving NDA methods, the data symbols *should* be modeled as random variables following the stochastic approach introduced in Section 2.3. Then, the likelihood function should be obtained by averaging the joint likelihood function using the known statistical distribution of the symbols. Additionally, the rest of unknown nuisance parameters can also be averaged out following a Bayesian approach. The resulting NDA ML criterion is referred to as the unconditional (or stochastic) maximum likelihood estimator in the literature (Section 2.3).

Because the difficult computation of the mentioned statistical averages, it is very common to consider that the signal-to-noise ratio of the received signal is very low (Section 2.4.1). Although this low-SNR assumption is not generally satisfied, it allows the development of reduced complexity synchronizers because the resulting schemes are usually quadratic in the observation.

A different interpretation of the NDA ML estimation is given in [Vaz00][Vaz01][Rib01a]. The new approach is based on the compression of the NDA ML function with respect to the vector of unknown symbols by adopting a linear estimation of these symbols. This approach is valuable because it unifies the different ML-based NDA solutions, namely the Low-SNR UML (Section 2.4.1), the Conditional ML (Section 2.4.2) and the Gaussian ML (Section 2.4.3).

In the following sections, the most important NDA synchronization techniques are briefly described and classified. For more information, the reader is referred to the excellent textbooks and historical reports on digital synchronization [Men97][Mey90][Gar88a][Gar90].

Timing Synchronization

One of the simplest algorithms exploiting the cyclostationarity property for timing estimation is the well-known Filter and Square Timing Recovery proposed in [Oer88] by M. Oerder and H. Meyr. This feedforward timing synchronizer is based on an explicit spectral line regeneration using quadratic processing. The Oerder&Meyr synchronizer was proved in [LS05a][Vaz00] to be

the low-SNR ML timing estimator if the carrier frequency error is uniformly distributed within the Nyquist bandwidth and the received symbols are uncorrelated. Likewise, the Oerder&Meyr synchronizer yields also the low-SNR ML solution in the absence of frequency errors as shown in [LS05a][Vaz00].

On the other hand, the application of the ML principle along with the approximation of low-SNR and some additional simplifications, has led to well-known closed-loop estimators such as the NDA Early-Late detector [Men97, Sec. 8.3.1.] and the Gardner's detector [Gar86a], which is shown to outperform the NDA Early-Late detector at high SNR.

A common problem of the existing NDA timing error detectors is the presence of the so-called self-noise (or pattern-noise) [Men97]. Self-noise is the timing jitter induced by the random received symbols. Indeed, this self-noise is a consequence of the adopted low SNR approximation. The occurrence of self-noise yields a high SNR floor on the timing estimation variance that might invalidate these techniques for the medium-to-high SNR range. This problem was addressed in detail in [And96]. In this paper, the authors proposed to pre-filter the received signal before detecting the timing error.

Finally, more recent research efforts have been concerned with timing recovery for Continuous Phase Modulation (CPM) [Men97][Vaz00]. These modulation schemes are attractive for their high spectral efficiency and constant envelope nature, which allows the use of low-cost, nonlinear amplifiers. The ML principle along with the low-SNR approximation has been also applied in this case, leading to timing recovery detectors very similar to those derived for a linear format.

Carrier-frequency synchronization

The structure of the frequency synchronizers highly depends on the magnitude of the maximum frequency offset as compared with the symbol rate. Early methods for feedback frequency recovery in the case of high frequency offset include quadricorrelators [Cah77][Gar88a] and dual filter detectors [Alb89][Gar88a], which have been proved to be equivalent solutions [Moe92]. The rotational detectors for estimating moderate frequency offsets with no timing uncertainty were introduced in [Mes79]. Other ad hoc schemes were proposed in [Sar88] and [Chu91] for the same problem.

The first rigorous treatment of the problem starting from a ML perspective can be found in [Gar90]. The frequency recovery methods developed under this framework also make use of the low-SNR approximation. However, the resulting low-SNR ML frequency error detectors become self-noise free if the timing is known. Self-noise appears only when the estimator does not use the timing information [Men97, Sec. 3.5.] and ad hoc techniques for eliminating this effect has been proposed in [Alb89] and [And93].

6.1.2 Signal Model

In this section, the signal model used in the context of digital communications is presented in detail. It is shown that most modulations of interest can be represented by means of the *linear, vectorial* model presented in Section 2.4. Let us start formulating the complex envelope of a generic digital modulation as follows:

$$y(t) = s(t - \tau; d_k) e^{j(\varphi + \omega t)} + w(t) \quad (6.1)$$

where $\{d_k\}$ are the information symbols conveyed in the transmitted signal $s(t)$, τ is the timing error within a symbol period $(-T/2, +T/2]$, φ and ω are the carrier phase and the carrier pulsation errors, respectively, and $w(t)$ is the *complex* AWGN term with double-sided power spectral density $S_w(f) = 2N_o$ Watts/Hz.¹

If the received signal is low-pass filtered in the Nyquist bandwidth $(-0.5/T_s, 0.5/T_s]$, the equivalent discrete signal model is given by

$$y(mT_s) = s(mT_s - \tau; d_k) e^{j(\varphi + \omega mT_s)} + w(mT_s) \quad (6.2)$$

where T_s is the sampling period. Under this sampling condition, the discrete noise $w(mT_s)$ remains white.

A first case of interest are those linear modulations admitting the following representation:

$$y(mT_s) = \sum_{k=-\infty}^{+\infty} d_k p(mT_s - kT - \tau) e^{j(\varphi + \omega mT_s)} + w(mT_s) \quad (6.3)$$

where $T = N_{ss}T_s$ is the symbol period and, $p(mT_s)$ are the samples of the pulse $p(t)$, which is supposed to last L symbol intervals. If we take $M \triangleq N_s N_{ss}$ samples to estimate the unknown parameters, the n -th observed vector

$$\mathbf{y}_n \triangleq [y(nT), \dots, y(nT + (M-1)T_s)]^T$$

is given by

$$\mathbf{y}_n = \mathbf{A}(\boldsymbol{\theta}) \mathbf{x}_n + \mathbf{w}_n \quad (6.4)$$

where the *transfer matrix*

$$\mathbf{A}(\boldsymbol{\theta}) \triangleq \begin{bmatrix} e^{j(\varphi + n\omega T)} p((L-1)T - \tau) & \dots & e^{j(\varphi + n\omega T)} p((1-N_s)T - \tau) \\ \vdots & \ddots & \vdots \\ e^{j(\varphi + (n+(M-1)/N_{ss})\omega T)} p((L+N_s-1)T - T_s - \tau) & \dots & e^{j(\varphi + (n+(M-1)/N_{ss})\omega T)} p(T - T_s - \tau) \end{bmatrix}$$

¹The in-phase and quadrature two-sided power spectral density is N_o W/Hz.

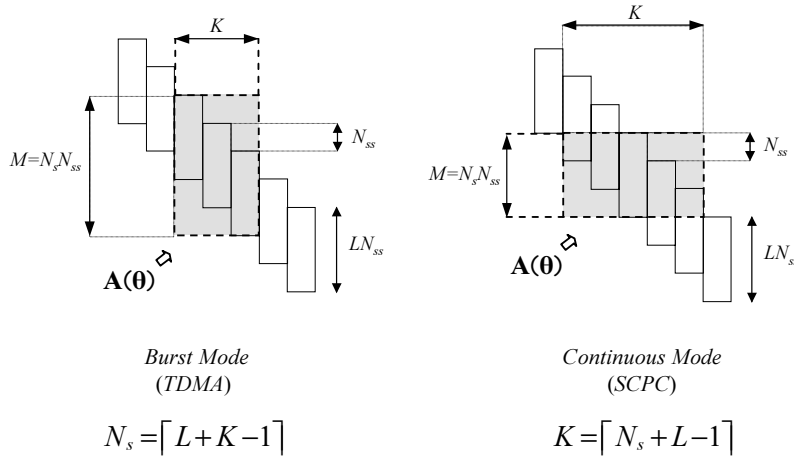


Figure 6.1: Structure of the transfer matrix $\mathbf{A}(\boldsymbol{\theta})$ in a burst or continuous transmission.

is a function of the normalized vector of parameters

$$\boldsymbol{\theta} \triangleq [\varphi, \tau/T, \omega T/2\pi]^T,$$

the vector $\mathbf{x}_n \triangleq [d_{n-L+1}, \dots, d_{n+N_s-1}]^T$ contains the observed data symbols, and the receiver noise \mathbf{w}_n is defined in the same way than the vector \mathbf{y}_n . The phase origin can be arbitrarily selected. For instance, a practical choice is the center of the observed interval.

In this section, we will focus on the timing and frequency estimation problems assuming that the signal phase is unknown. In that case, the term $e^{j\varphi}$ can be integrated into the nuisance parameter vector \mathbf{x}_n and non-coherent (i.e., quadratic) estimation techniques are adopted.

Implicitly, a single channel per carrier (SCPC) system is assumed throughout this thesis in which a continuous, infinite stream of symbols is received (6.3). In that case the initial $L - 1$ and final $L - 1$ symbols are partially observed and, consequently, the modulation matrix $\mathbf{A}(\boldsymbol{\theta})$ has $N_s + L - 1$ columns and only $N_s N_{ss}$ rows. Therefore, oversampling ($N_{ss} > 1$) is normally necessary to have more samples than unknowns, i.e.,

$$N_s N_{ss} > N_s + L - 1.$$

This condition is usually a requirement to cancel out the disturbance of the modulation and yield self-noise free estimates of $\boldsymbol{\theta}$. The structure of matrix $\mathbf{A}(\boldsymbol{\theta})$ is depicted in Fig. 6.1 (right-hand side) and its Grammian is a function of τ and ω as indicated next

$$[\mathbf{A}(\boldsymbol{\theta})\mathbf{A}^H(\boldsymbol{\theta})]_{m_1, m_2} = e^{j\omega(m_1 - m_2)T_s} \sum_{k=-\infty}^{\infty} p(m_1 T_s - kT - \tau) p(m_2 T_s - kT - \tau).$$

On the other hand, a burst of K symbols is transmitted in a time-division multiple access (TDMA) system. In that case, the observation is composed of $(K + L) N_{ss} - 1$ non-zero samples

and, thus, oversampling is not strictly necessary if the received burst is integrally processed. In a TDMA system the matrix $\mathbf{A}(\boldsymbol{\theta})$ is Sylvester (see Fig. 6.1) and, if the transmitted pulse is sampled without aliasing, we have that

$$[\mathbf{A}^H(\boldsymbol{\theta})\mathbf{A}(\boldsymbol{\theta})]_{k_1, k_2} = R_{pp}((k_1 - k_2)T)$$

where $R_{pp}(\Delta t) \triangleq \int p(t)p(t + \Delta t)dt$ is the pulse autocorrelation. Therefore, $\mathbf{A}^H(\boldsymbol{\theta})\mathbf{A}(\boldsymbol{\theta})$ does not depend on $\boldsymbol{\theta}$.

Synchronization algorithms for SCPC systems has to cope with the partial observation of the initial and final symbols. Optimal synchronizers weight the observed samples taking into account that the initial and final symbols provide less information about $\boldsymbol{\theta}$ than the central ones. The larger is the observation time (N_s) the less significant is this “edge effect”. This problem is very relevant, for example, in the carrier phase estimation problem studied in Section 6.2. Asymptotically, the “edge effect” is negligible and the synchronization techniques for SCPC systems are identical to those derived for TDMA systems. Thus, in the asymptotic case synchronizers can be designed considering uniquely the central column of $\mathbf{A}(\boldsymbol{\theta})$ (Section 7.4.4).

The linear model in equation (6.3) can be extended to encompass more sophisticated scenarios such as multicarrier schemes, multiple access systems, space-time transmissions, or binary CPM modulations on account of the Laurent’s decomposition [Lau86][Men95]. In all these cases, the received signal can be expressed as the superposition of J linearly modulated signals as follows

$$\mathbf{y} = \sum_{j=1}^J \mathbf{A}_j(\boldsymbol{\theta}_j) \mathbf{x}_j + \mathbf{w} = \mathbf{A}(\boldsymbol{\theta}_1, \dots, \boldsymbol{\theta}_J) \mathbf{x} + \mathbf{w}$$

with

$$\begin{aligned} \mathbf{A}(\boldsymbol{\theta}_1, \dots, \boldsymbol{\theta}_J) &\triangleq [\mathbf{A}_1(\boldsymbol{\theta}_1), \dots, \mathbf{A}_J(\boldsymbol{\theta}_J)] \\ \mathbf{x} &\triangleq [\mathbf{x}_1^T, \dots, \mathbf{x}_J^T]^T \end{aligned}$$

where the index n is omitted for simplicity and $\boldsymbol{\theta}_j$ stands for the parameters of the j -th user in case of a multiple access system. The basic difference with respect to (6.3) is that the J signals are usually *non-orthogonal* and, thus, they interfere each other if we deal with space-time transmissions [Vil03c], asynchronous CDMA users or, binary CPM signals. Moreover, the J pseudo-pulses of the CPM signal suffer from intersymbol interference (ISI) at their matched filter output. All these terms of interference introduce an additional noisy component affecting the estimator performance at high SNR and yielding the so-called self-noise.

6.1.3 Open-Loop Timing Synchronization

In Chapter 3, the formulation of the optimal open-loop second-order estimator was addressed. In that chapter, the parameters of interest were modeled as random variables with known probability density function $f_{\boldsymbol{\theta}}(\boldsymbol{\theta})$. Then, the estimator coefficients were optimized averaging the

estimator bias and variance with respect to the prior $f_{\theta}(\boldsymbol{\theta})$. The Bayesian expectation was solved analytically for the problem of frequency estimation in Section 3.4 and some simulations were presented to illustrate the theory of feedforward quadratic estimation.

Unfortunately, in most problems, the expectation with respect to $f_{\theta}(\boldsymbol{\theta})$ must be solved numerically as, for example, when addressing the problem of timing synchronization. To overcome this drawback, in this section we propose to process the received signal in the frequency domain where the timing error appears as a frequency shift. In that way, the formulation in Section 3.4 can be applied to both the frequency and timing estimation problems.

Let \mathbf{z} be the DFT of the observed vector \mathbf{y} , which is computed as

$$\mathbf{z} \triangleq \mathbf{F}\mathbf{y} = \mathbf{F}\mathbf{A}(\boldsymbol{\theta})\mathbf{x} + \mathbf{F}\mathbf{w},$$

where \mathbf{F} stands for the unitary $M \times M$ DFT matrix defined as follows:

$$\mathbf{F} \triangleq \frac{1}{\sqrt{M}} \exp\left(-j\frac{2\pi}{M}\mathbf{d}_M\mathbf{d}_M^T\right)$$

with $\mathbf{d}_M \triangleq [-M/2, \dots, M/2 - 1]^T$. Notice that MT_s must be greater than the burst duration plus twice the maximum delay to prevent the existence of temporal aliasing.

In the frequency domain, the transfer matrix can be written as

$$\mathbf{B}(\boldsymbol{\theta}) \triangleq \mathbf{F}\mathbf{A}(\boldsymbol{\theta}) = e^{j\varphi}\mathbf{E}_2(\tau)\mathbf{F}\mathbf{E}_1(\nu)\mathbf{A}(\mathbf{0}) \quad (6.5)$$

with

$$\begin{aligned} \mathbf{E}_1(\nu) &\triangleq \text{diag}\left[\exp\left(j2\pi\frac{\nu}{N_{ss}}\mathbf{d}_M\right)\right] \\ \mathbf{E}_2(\tau) &\triangleq \text{diag}\left[\exp\left(-j2\pi\frac{\tau N_{ss}}{M}\mathbf{d}_M\right)\right] \end{aligned}$$

the diagonal matrices accounting for the frequency and timing error, normalized with respect to the symbol period T . In that way, the observation \mathbf{z} exhibits the same phasorial dependence on the three parameters φ , τ and ν . Therefore, the results in Appendix 3.D can be used to obtain a closed-form expression for the optimal quadratic open-loop timing synchronizer.

Notice that optimal estimators can be obtained from $\mathbf{z} = \mathbf{F}\mathbf{y}$ since \mathbf{F} is a unitary transformation that can always be inverted –if necessary– by the estimator matrix \mathbf{M} without having noise enhancement. Moreover, the transformation does not change the noise statistics if the original Gaussian noise \mathbf{w} is spectrally white.

To conclude, it is worth realizing that (6.5) is only held if all the received pulses are entirely observed. Otherwise, those partially observed pulses cannot be interpolated from the vector of samples \mathbf{y} because they do not satisfy the Nyquist criterion. Thus, the above expression can be applied to design open-loop estimators if the entire burst –including the pulse tails– is captured and processed in a TDMA system or, alternatively, if the observation time is sufficiently large to neglect the “edge effect” in SCPC systems (Section 6.1.2).

6.1.4 Closed-Loop Analysis and Optimization

In Chapter 4, the optimum second-order *small-error* estimator was deduced and then simulated for the frequency estimation problem. The solution therein can be adopted to design the discriminator of NDA timing and frequency closed-loop synchronizers. In this manner, the discriminator coefficients are selected to minimize the steady-state variance at the discriminator output. However, this optimization criterion is not taking into account that the discriminator output is further *lowpass filtered* by the loop impulse response. For example, an exponential filtering is carried out in case of a first-order closed-loop. When the discriminator output is temporally uncorrelated, this standard procedure is globally optimal and the estimator variance is computed as the discriminator variance divided by the effective loop filter memory $N \approx 0.5/B_n$ where B_n is the noise equivalent loop bandwidth. This case corresponds to the closed-loop estimator in Section 2.5.1 processing independent blocks \mathbf{z}_n . However, if the detected errors are correlated because overlapped blocks of the received signal are processed, the estimator variance is no longer divided by N and the standard procedure for designing the discriminator is suboptimal. Remember that overlapping is generally required to have efficient closed-loop estimators (see Proposition 2.1).

In this section, the small-error variance of any quadratic NDA closed-loop estimator is formulated analytically. This expression is then optimized to find the optimal discriminator coefficients. Some numerical results for the timing estimation problem are provided comparing the aforementioned design criteria. Notice that the formulation is absolutely general and can be applied to other uniparametric and multiparametric second-order estimation problems. Also, the results in this section are useful in the context of open-loop estimation (Chapter 3) if the parameter estimates are post-filtered. In that case, the Bayesian expectation should be incorporated into all the following expressions.

The output of any quadratic discriminator of $\boldsymbol{\alpha} = \mathbf{g}(\boldsymbol{\theta})$ can be expressed as

$$\mathbf{e}_n \triangleq \hat{\boldsymbol{\alpha}}_n - \mathbf{g}(\boldsymbol{\theta}_o) = \mathbf{M}^H (\hat{\mathbf{r}}_n - \mathbf{r}_o) \quad (6.6)$$

where \mathbf{M} are the discriminator coefficients under design, $\hat{\mathbf{r}}_n$ is the (vectorized) sample covariance matrix for the n -th observed block and, \mathbf{r}_o is the expected value of $\hat{\mathbf{r}}_n$ for any value of n . The sequence \mathbf{e}_n is strict-sense stationary with zero mean and covariance $\mathbf{M}^H \mathbf{Q}_0 \mathbf{M}$ where

$$\mathbf{Q}_0 \triangleq E \left\{ (\hat{\mathbf{r}}_n - \mathbf{r}_o) (\hat{\mathbf{r}}_n - \mathbf{r}_o)^H \right\}$$

is the covariance matrix of the quadratic observation $\hat{\mathbf{r}}_n$ (3.10). The meaning of subindex in \mathbf{Q}_0 will be explained next. Let us remind the reader that the discriminator coefficients minimizing the variance of \mathbf{e}_n were found in Section 4.2.

Let us consider now that h_n is the loop infinite impulse response. In that case, the estimation

errors are given by

$$\boldsymbol{\varepsilon}_n \triangleq \sum_{k=0}^{\infty} h_k \mathbf{e}_{n-k} = \sum_{k=0}^{\infty} h_k \mathbf{M}^H (\hat{\mathbf{r}}_{n-k} - \mathbf{r}_o) = \mathbf{M}^H \sum_{k=0}^{\infty} h_k (\hat{\mathbf{r}}_{n-k} - \mathbf{r}_o)$$

that is a strict-sense stationary zero-mean sequence with covariance

$$E \{ \boldsymbol{\varepsilon}_n \boldsymbol{\varepsilon}_n^H \} = \mathbf{M}^H \left(\sum_{m=-\infty}^{\infty} R_{hh} [m] \mathbf{Q}_m \right) \mathbf{M}$$

where $R_{hh} [m] \triangleq \sum_{k=m}^{\infty} h_k h_{k-m}$ is the autocorrelation function of the filter h_n and

$$\mathbf{Q}_m \triangleq E \left\{ (\hat{\mathbf{r}}_n - \mathbf{r}_o) (\hat{\mathbf{r}}_{n-m} - \mathbf{r}_o)^H \right\}$$

stands for the “vectorial autocorrelation function” of the quadratic observation $\hat{\mathbf{r}}_n$ evaluated at the m -th lag. Thus, \mathbf{Q}_0 stands for \mathbf{Q}_m at $m = 0$.

Notice that \mathbf{Q}_m is defined for lags $|m| \leq D$ where D stands for the number of consecutive statistically-dependent blocks. In that way, the covariance of the estimation error is

$$E \{ \boldsymbol{\varepsilon}_n \boldsymbol{\varepsilon}_n^H \} = \mathbf{M}^H \left(\sum_{m=-D}^D R_{hh} [m] \mathbf{Q}_m \right) \mathbf{M} \approx E_h \mathbf{M}^H \left(\sum_{m=-D}^D \mathbf{Q}_m \right) \mathbf{M}$$

where $E_h \triangleq R_{hh} [0] = \sum_{k=0}^{\infty} h_k^2$ is the filter impulse response energy. In the last approximation, we have taken into account that the bandwidth of h_n is very small and, therefore, $R_{hh} [m]$ is approximately flat for $|m| \leq D$. Finally, notice that $E_h = 1/N \approx 2B_n$ where N and B_n are the effective loop memory and the noise equivalent loop bandwidth, respectively, assuming that $\sum_{k=0}^{\infty} h_k = 1$ is verified to have unbiased estimates (Section 2.5.2).

In the last equation, the variance of any quadratic (unbiased) closed-loop estimator is given by

$$E \{ \boldsymbol{\varepsilon}_n \boldsymbol{\varepsilon}_n^H \} = \mathbf{M}^H \mathbf{Q}_{opt} \mathbf{M}$$

where the fourth-order matrix \mathbf{Q}_{opt} is given by

$$\mathbf{Q}_{opt} \triangleq \sum_{m=-D}^D R_{hh} [m] \mathbf{Q}_m \approx E_h \sum_{m=-D}^D \mathbf{Q}_m = \frac{1}{N} \sum_{m=-D}^D \mathbf{Q}_m.$$

and, therefore, the optimal solution is the one deduced in Section 4.2 with $\mathbf{Q}_o = \mathbf{Q}_{opt}$ instead of $\mathbf{Q}_o = \mathbf{Q}_0$. Thus, the optimal and original second-order discriminators are

$$\begin{aligned} \mathbf{M}_{opt} &= \mathbf{Q}_{opt}^{-1} \mathbf{D}_r (\mathbf{D}_r^H \mathbf{Q}_{opt}^{-1} \mathbf{D}_r)^{\#} \mathbf{D}_g^H \\ \mathbf{M}_0 &= \mathbf{Q}_0^{-1} \mathbf{D}_r (\mathbf{D}_r^H \mathbf{Q}_0^{-1} \mathbf{D}_r)^{\#} \mathbf{D}_g^H, \end{aligned}$$

respectively.

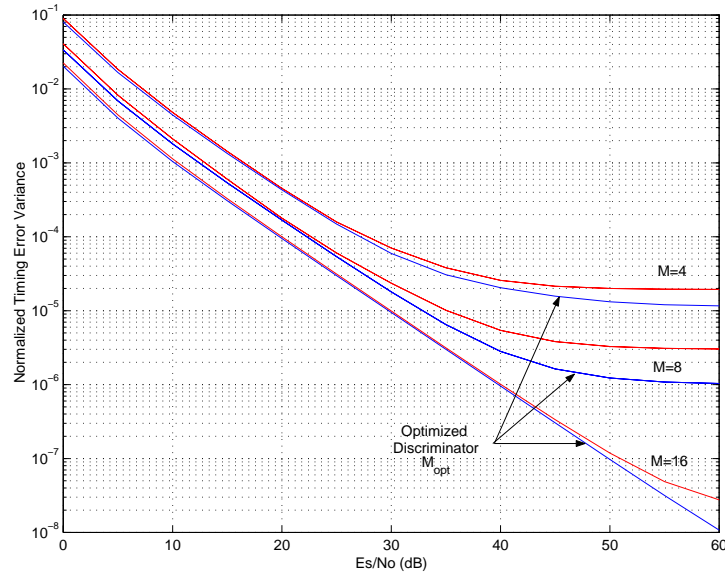


Figure 6.2: Timing error variance with and without loop optimization for different number of samples M in case of the QPSK modulation with roll-off 0.1 and $N_{ss} = 2$. The same curves are obtained for QAM and MPSK.

If $R_{ee}[m]$ and $S_{ee}(f) = \sum_m R_{ee}[m]e^{-j2\pi fm}$ stand for the autocorrelation and the power spectrum of the error sequence \mathbf{e}_n in (6.6), we can affirm that the optimal discriminator \mathbf{M}_{opt} minimizes $S_{ee}(0) = \sum_m R_{ee}[m]$ whereas the original discriminator \mathbf{M}_0 minimized $R_{ee}[0] = \int_{-1/2}^{1/2} S_{ee}(f)df$. This means that the optimal discriminator should filter out the very low-frequency errors and let the loop filter to cancel out the high-frequency errors. This fact becomes relevant at high SNR because the self-noise is actually a highpass disturbance.

Unfortunately, this desirable aim is severely limited by the unbiased constraint and minor gains have been observed for practical SNRs, at least for the symbol synchronization problem. In Fig. 6.2 and 6.3, it is shown how the self-noise can be reduced at high SNR in case of MPSK and QAM transmissions with small roll-off pulse shaping. On the other hand, if some bias is accepted, the discriminator could adopt a more highpass response in order to reduce the ultimate variance in low-SNR scenarios following the Bayesian formulation in Chapter 3.

6.1.5 Numerical Results

The carrier estimation problem was adopted in Sections 3.4 and 4.5 to illustrate the theory of second-order optimal estimation in the field of digital communications. Simulations were provided comparing the optimal solution with the classical ML-based estimators as well as the

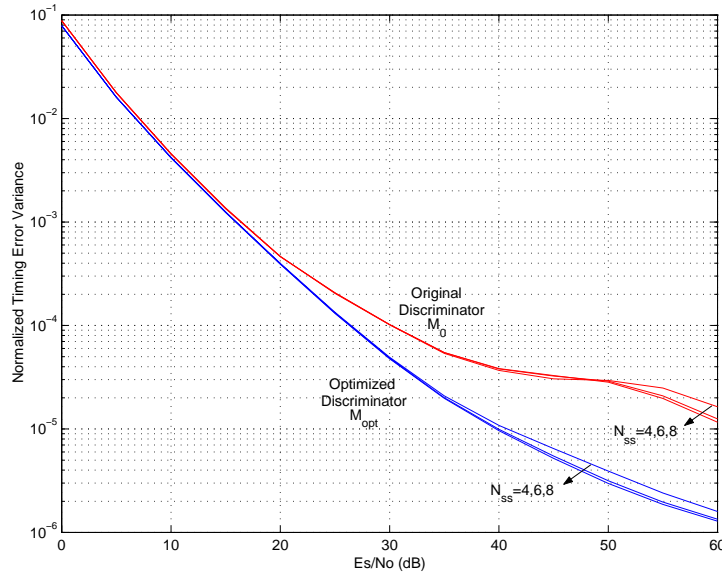


Figure 6.3: Timing error variance with and without loop optimization for N_{ss} equal to 4, 6 and 8 in case of the QPSK modulation with roll-off 0.1 and $M=4$.

unconditional and modified CRB. To complement these results, some simulations are presented in this section for the problem of digital clock recovery.

Closed-loop timing synchronization

The optimal second-order timing estimator is compared to the GML and the low-SNR UML. The NDA Early&Late [Men97, Sec. 8.5.2.], Gardner's [Gar86a], Oerder&Meyr's [Oer88] synchronizers are also simulated because they are actually the most usual timing synchronizers in practical implementations (Fig. 6.4 and 6.5). Notice that the three algorithms are based on the low-SNR approximation and, therefore, they suffer from self-noise at high SNR. A first-order closed-loop is simulated with the (normalized) noise equivalent loop bandwidth set to $B_n = 5 \times 10^{-3}$ (i.e., $N = 100$ symbols). All the E_s/N_0 values are simulated assuming that the small-error condition is verified. Finally, the CML estimator is not simulated because, in the considered scenario, there are more nuisance parameters than observed samples, i.e., $M = 4$ and $K = 11$.

The Gaussian assumption is found to yield optimal timing synchronizers for those linear modulations, such as QAM and MPSK, for all the simulated SNR (Fig. 6.4 and 6.5). On the other hand, simulations for the MSK modulation have shown a minor improvement for medium-to-high SNRs [Vil01b], as illustrated in Fig. 6.6. In the same plot, the optimal fourth-order

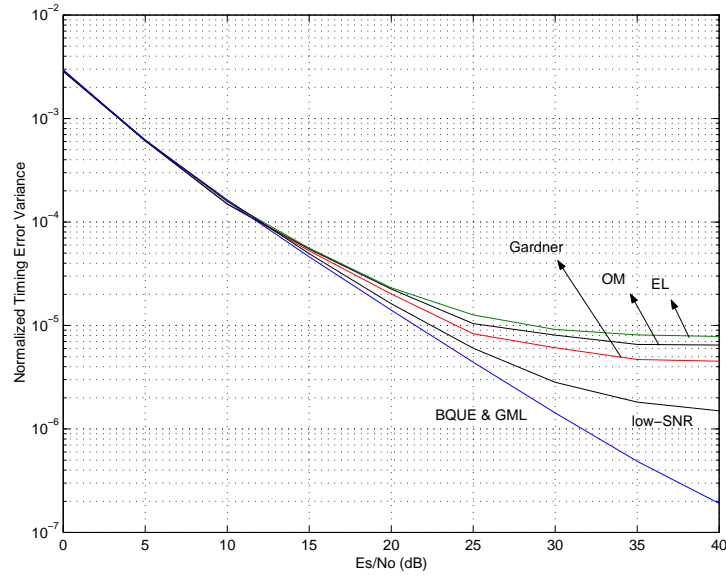


Figure 6.4: Normalized timing variance for the low-SNR ML and GML estimators as well as the EL (Early&Late), OM (Order&Meyr) and Gardner’s symbol synchronizers. The simulation parameters are; 16-QAM, roll-off 0.75, $N_{ss}=2$ ($N_{ss}=4$ for the Order&Meyr), $M = 2N_{ss}$ and, $B_n = 5 \cdot 10^{-3}$. The shaping pulse and the associated matched filter are truncated at $\pm 5T$.

detector designed in [Vil01b] is simulated showing that higher-order methods are only able to outperform second-order techniques at high SNR.

Open-loop timing synchronization

Some simulations are also presented in Figs. 6.7-6.12 for the open-loop timing synchronizer. The second-order minimum variance (\mathbf{M}_{var}) and MMSE (\mathbf{M}_{mse}) estimators proposed in Section 3 are compared with the closed-loop estimator formulated in Section 4. The timing is estimated from a burst of $K = 4$ symbols. Simulations are run for the 16-QAM and MSK modulations. In the first case the transmitted pulse is a square-root raised cosine with roll-off 0.75 and duration $5T$. The sampling rate is twice the symbol rate, i.e., $N_{ss} = 2$. The normalized timing error is modeled as a uniform random variable in the interval $\pm\Delta/2$. Notice that in a TDMA system the range of Δ is extended to $\pm N_s$ with N_s the burst duration in symbols. The reason is that we are actually dealing with a semiblind estimation problem since those symbols before and after the burst are known to be null.

In Fig. 6.7 the normalized MSE is plotted as a function of the timing error for $\Delta = 1$, $K = 4$ and $E_s/N_0=10$ dB. It can be shown that the MMSE is able to outperform the minimum variance estimator because it is not forced to yield unbiased estimates within the prior range,

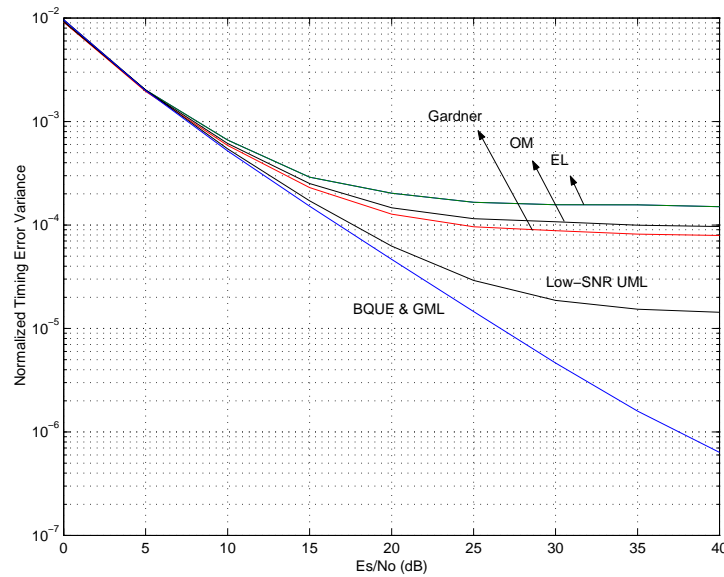


Figure 6.5: Normalized timing variance for the low-SNR ML and GML estimators as well as the EL (Early&Late), OM (Order&Meyr) and Gardner’s symbol synchronizers. The simulation parameters are; 16-QAM, roll-off 0.25, $N_{ss}=2$ ($N_{ss}=4$ for the Order&Meyr), $M = 2N_{ss}$ and, $B_n = 5 \cdot 10^{-3}$. The shaping pulse and the associated matched filter are truncated at $\pm 5T$.

i.e., $\pm\Delta/2 = \pm 1/2$. On the other hand, the closed-loop estimator is optimized for $\tau = 0$ but its performance degrades rapidly when the timing error approaches the prior limits at $\tau = \pm\Delta/2$.

The estimators mean response as well as their squared bias is simulated in Fig. 6.8 and Fig. 6.9, respectively. It is shown that bias is easily cancelled for $\Delta = 1$ since it is a small fraction of the burst duration, which is equal to 8 symbols in the simulated scenario.

Some additional conclusions can be drawn from these simulations:

- In noisy scenarios, the loss incurred by open-loop estimators becomes negligible when compared to the performance of closed-loop estimators (Fig. 6.7). On the other hand, closed-loop estimators are superior at high SNR as shown in Fig. 6.10.
- The minimum variance and MMSE open-loop estimators converge when the SNR is augmented for the MSK modulation (Fig. 6.11). On the other hand, self-noise is observed at high SNR for the 16-QAM constellation (Fig. 6.12). In that case, the MMSE estimator outperforms the minimum variance solution because it introduces some bias in order to reduce the self-noise variance.

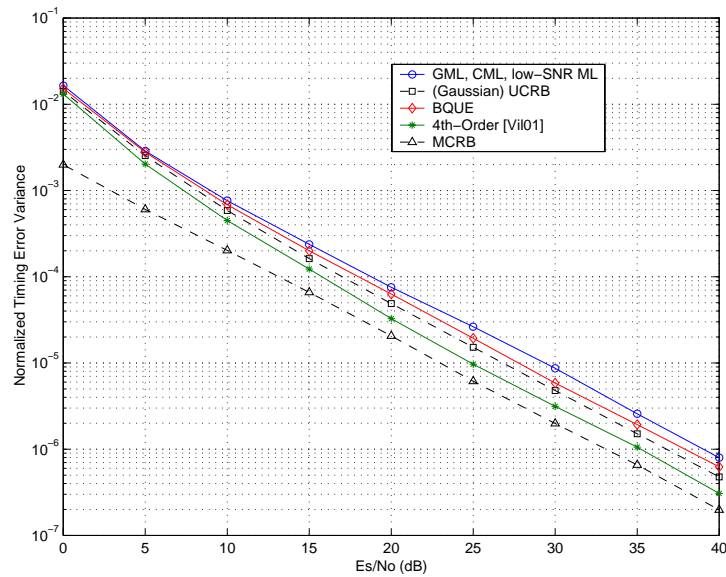


Figure 6.6: Normalized timing variance for the ML-based estimators for the MSK modulation with $N_{ss}=2$, $M=4$ and, $B_n = 5 \cdot 10^{-3}$.

- The Gaussian assumption leads to suboptimal open-loop synchronizers at high SNR (Figs. 6.11 and 6.12). Regarding the MSK simulation, the Gaussian assumption avoids having self-noise free timing estimates (Fig. 6.11).

Some of the results in this section were presented for the first time in the IEEE International Workshop on Statistical Signal Processing that was held in Singapore in 2001 [Vil01a]. This work was further elaborated in [Vil02b] and presented in the IEEE Global Communications Conference that was held in Taipei in 2002:

- “Best Quadratic Unbiased Estimator (BQUE) for Timing and Frequency Synchronization”. J. Villares, G. Vázquez. Proceedings of the *11th IEEE International Workshop on Statistical Signal Processing (SSP01)*. pp. 413-416. Singapore. August 2001.
- “Sample Covariance Matrix Based Parameter Estimation for Digital Synchronization”. J. Villares, G. Vázquez. Proceedings of the *IEEE Global Communications Conference 2002 (Globecom 2002)*. November 2002. Taipei (Taiwan).

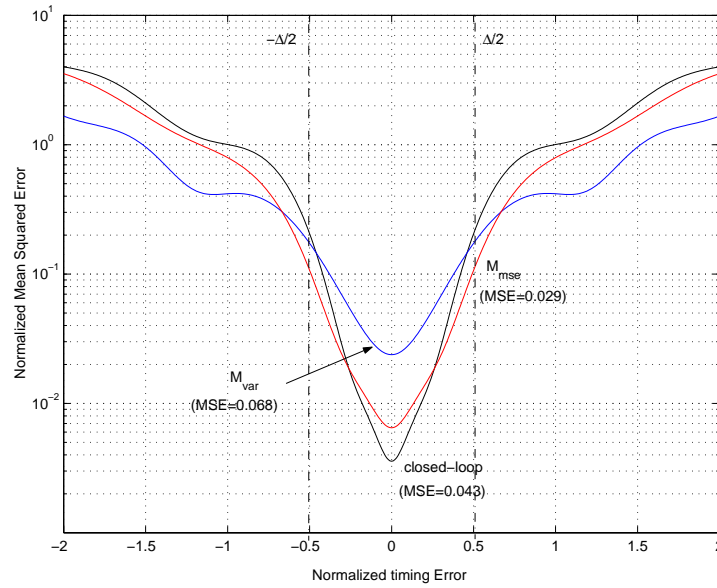


Figure 6.7: Normalized timing MSE for the MMSE, minimum variance and closed-loop second-order estimators for $K = 4$ and $E_s/N_0=10\text{dB}$. The average MSE for the three estimators is included inside round brackets.

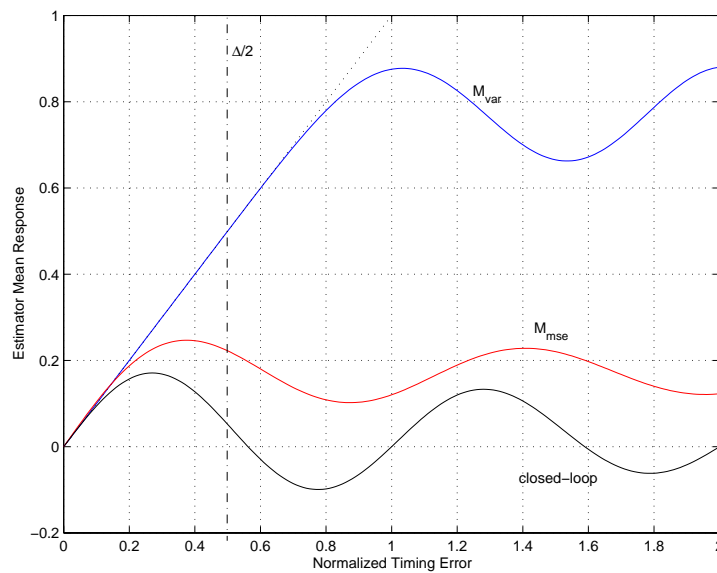


Figure 6.8: Estimation mean response for the MSE for the MMSE, minimum variance and closed-loop second-order estimators for $K = 4$ and $E_s/N_0=10\text{dB}$.

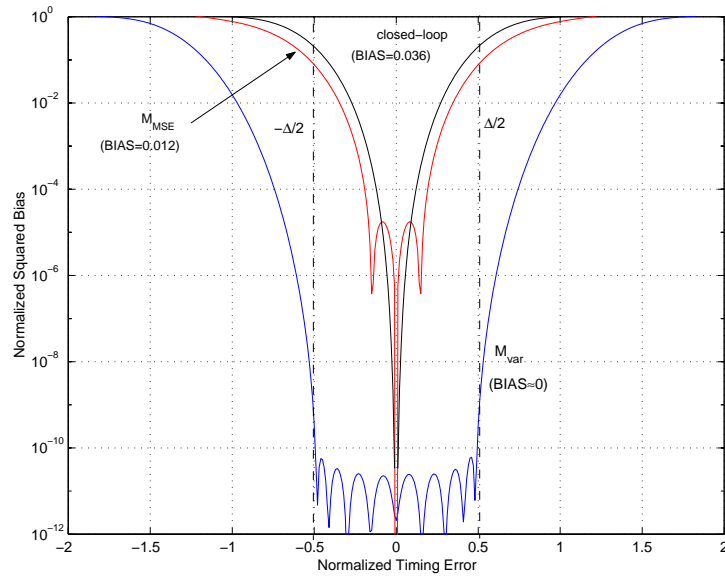


Figure 6.9: Normalized timing squared bias for the MMSE, minimum variance and closed-loop second-order estimators for $K = 4$ and $E_s/N_0=10\text{dB}$. The average BIAS for the three estimators is included inside round brackets.

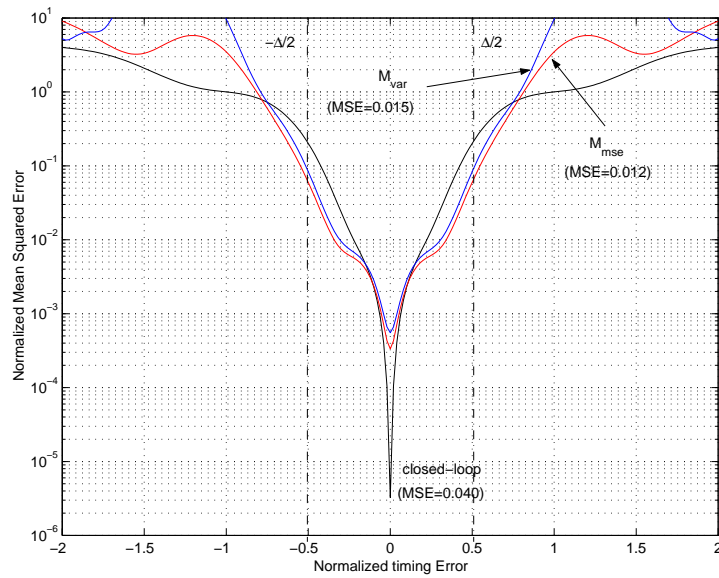


Figure 6.10: Normalized timing MSE for the MMSE, minimum variance and closed-loop second-order estimators for $K = 4$ and $E_s/N_0=40\text{dB}$. The average MSE for the three estimators is included inside round brackets.

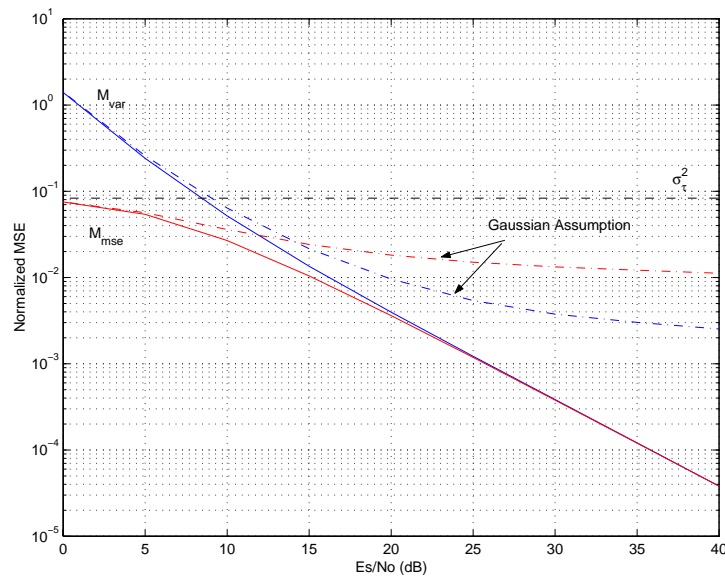


Figure 6.11: Normalized timing MSE for the MMSE (M_{mse}) and minimum variance (M_{var}) second-order estimators for the MSK modulation when $K = 4$ and $\Delta = 1$. The suboptimal estimators deduced under the Gaussian assumption are also plotted.

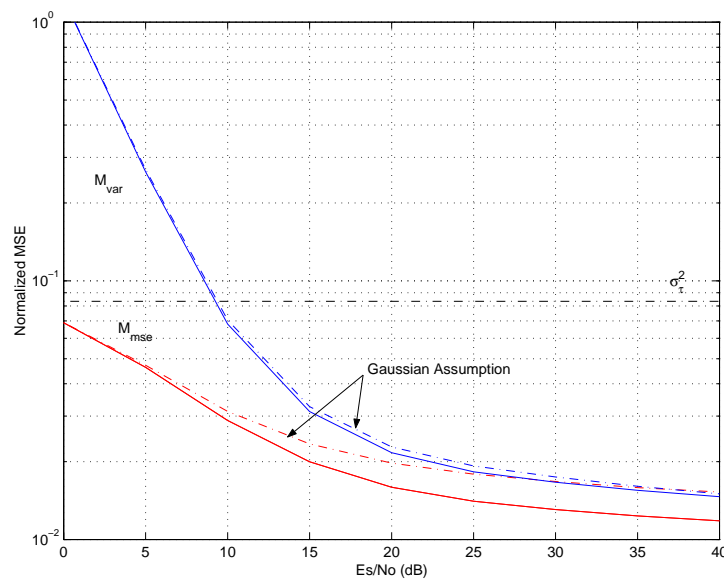


Figure 6.12: Normalized timing MSE for the MMSE (M_{mse}) and minimum variance (M_{var}) second-order estimators for the 16-QAM modulation when $K = 4$ and $\Delta = 1$. The suboptimal estimators deduced under the Gaussian assumption are also plotted.

6.2 Carrier Phase Synchronization of Noncircular Modulations

Coherent demodulation of continuous phase modulations (CPM) requires knowledge of the phase and frequency of the received carrier. Self-synchronizing techniques are normally preferred because they avoid the transmission of inefficient training sequences. Moreover, non-data-aided (NDA) algorithms are more appropriate in noisy scenarios because they do not rely on unreliable decisions but on the statistical structure of the received waveform [Men97].

In the synchronization field, the Laurent's expansion (LE) has been frequently used to derive synchronization techniques for CPM receivers [Men97][Vaz00][Mor00]. The LE is interesting because it allows expressing the non-linear CPM format as the summation of a finite number of pulse amplitude modulated (PAM) signals [Lau86][Men95]. Thus, all the extensive literature on synchronization and parameter estimation for linearly modulated signals can be reused [Rib01b]. On the other hand, the LE allows building scalable schemes considering uniquely the most powerful components of the decomposition [Mor00].

Focusing on the carrier phase estimation problem, Mengali et al. derived in [Men97, Sec. 6.6.2] the ML NDA carrier phase synchronizer under the low SNR assumption for MSK-type modulations (e.g., MSK, LREC, LRC, GMSK) [Men97]. The obtained solution was shown to be *quadratic* in the data. This is actually a unique feature of MSK-type signals because higher order techniques are required for NDA carrier phase synchronization in case of linear modulations [Ser01][Moe94] as well as general CPM signals.

Based on the LE, this property can be justified because the pseudo-symbols are not *circular* [Pic94] in case of MSK-type modulations and, therefore, the square of the received signal is not zero-mean and offers information about the parameter of interest [Moe94]. Finally, note that the N -th power synchronizer studied in [Moe94] can still be applied to MSK-type modulations although it will be inefficient at low SNR, as stated previously, and will not attain the Cramér-Rao bound (CRB) either when the SNR tends to infinity because CPM modulations suffer from intersymbol interference (ISI).

From this background, in Section 6.2.2, the low-SNR ML estimator has been reformulated using vectorial notation and the Laurent's decomposition. The subsequent analysis of the low-SNR approximation at high SNR in Section 6.2.3 reveals the existence of a significant variance floor due to the so-called *self-noise*, that is, the variability caused by the own modulation in NDA schemes. This floor is inappreciable when the observation is sufficiently large but it is determinant for short samples.

This drawback motivated the design of *second-order self-noise free* schemes minimizing the aggregated contribution of thermal plus pattern noise for a given SNR. The proposed second-order optimal synchronizer is deduced in Section 6.2.4 and its asymptotic study is presented in

Section 6.2.5 concluding that, with partial-response signals, some data patterns make the carrier phase unidentifiable if self-noise corrupted estimates are not tolerated. The estimator failure has been related to the singularity of the modulating matrix in partial-response signals. Anyway, although the above circumstance might slow down the parameter acquisition in a closed-loop implementation, self-noise free estimates are guaranteed after convergence. To conclude, the above statements are checked via simulation in Section 6.2.6.

The results of this section were presented in the IEEE International Conference on Communications that was held in Paris in 2004 [Vil04b]:

- “Self-Noise Free Second-Order Carrier Phase Synchronization of MSK-Type Signals”, J. Villares, G. Vázquez, Proc. of the *IEEE International Conference on Communications* (ICC 2004). June 2004. Paris (France).

6.2.1 Signal Model

The Laurent’s expansion (LE) allows the representation of *binary* CPM signals as the sum of a few PAM waveforms [Lau86][Men97]. This transformation is adopted in this section in order to formulate carrier phase synchronizers for the *nonlinear* CPM format. It was shown in Section 6.1.2 that the complex envelope of the *sampled* CPM signal is given by

$$\mathbf{y} = e^{j\theta_o} \sum_{j=0}^{J-1} \mathbf{A}_j \mathbf{x}_j + \mathbf{w} = e^{j\theta_o} \mathbf{A} \mathbf{x} + \mathbf{w} \quad (6.7)$$

where θ_o is the unknown carrier phase that must be estimated, \mathbf{x}_j the pseudo-symbols from the j -th component of the Laurent’s expansion having contribution into the observation \mathbf{y} , \mathbf{A}_j the associated modulating matrix formed from the j -th pseudo-pulse coefficients and, \mathbf{w} the vector of AWG noise. The J components of the LE expansion are stacked in the following manner:

$$\begin{aligned} \mathbf{x} &= [\mathbf{x}_0^T, \dots, \mathbf{x}_{J-1}^T]^T \\ \mathbf{A} &= [\mathbf{A}_0, \dots, \mathbf{A}_{J-1}]. \end{aligned}$$

In order to simplify the study, the following assumptions are taken in the following; 1) the receiver has perfect timing and frequency-offset synchronization; 2) the CPM modulator has achieved the steady-state; 3) the focus is on MSK-type signals for which the modulation index is $h = 0.5$ and hence the carrier phase shifts are equal to $\pm\pi/2$; 4) $\theta_o \in (-\pi/2, \pi/2]$ in order to avoid the inherent ambiguity of quadratic methods [Men97]. Additionally, the study is carried out for a continuous transmission system as explained in Section 6.1.2. This point is specially relevant because some of the concluding remarks are a consequence of the continuous mode model.

6.2.2 NDA ML Estimation in Low-SNR Scenarios

In this section, the ML principle is applied to find the optimum estimator of θ_o when the SNR is asymptotically low. As it was stated in Section 2.3, the ML estimator is the maximizer of the following cost function:

$$f_{\mathbf{y}}(\mathbf{y}; \theta) = CE_{\mathbf{x}} \left\{ \exp \left(-\sigma_w^{-2} \|\mathbf{y} - e^{j\theta} \mathbf{A}\mathbf{x}\|^2 \right) \right\} \propto E_{\mathbf{x}} \left\{ \exp \left(\sigma_w^{-2} \chi(\mathbf{y}; \mathbf{x}, \theta) \right) \right\} \quad (6.8)$$

where C is an irrelevant constant, $E_{\mathbf{x}}\{\cdot\}$ the expectation with respect to the pseudo-symbols distribution, σ_w^2 the variance of the noise samples and

$$\chi(\mathbf{y}; \mathbf{x}, \theta) \triangleq 2 \operatorname{Re}(e^{-j\theta} \mathbf{x}^H \mathbf{A}^H \mathbf{y}) \quad (6.9)$$

is the term in the exponent of (6.8) that depends on θ .

Unfortunately, the expectation with respect to \mathbf{x} normally complicates the calculation of a closed-form for $f_{\mathbf{y}}(\mathbf{y}; \theta)$. To overcome this obstacle, the likelihood function (6.8) is usually evaluated assuming that the SNR tends to zero, that is, $\sigma_w^2 \rightarrow \infty$. Following this reasoning, Mengali deduced in [Men97, Sec. 6.6.2] the *low-SNR* ML estimator of θ_o directly from the angular signal model in case of MSK-type signals.

Next, an alternative deduction is provided from the vectorial model in Section 6.2.1. In contrast to [Men97, Sec. 6.6.2], the obtained ML solution is exact even if the observation is short. Notice too that [Men97, Sec. 6.6.2] approximates the squared CPM signal (averaged with respect to the data) by means of the first harmonic of its Fourier series in order to yield a low-cost implementation based on transversal filtering. It can be shown that this approximation is only exact for LREC signals in which the frequency pulse is rectangular.

The deduction is initiated expanding the logarithm of (6.8) in a Taylor series at $\sigma_w^{-2} = 0$, having that

$$\ln f_{\mathbf{y}}(\mathbf{y}; \theta) \simeq \frac{1}{2} \sigma_w^{-4} E_{\mathbf{x}} \left\{ \chi^2(\mathbf{y}; \mathbf{x}, \theta) \right\}$$

except for some irrelevant additive constants (see Section 2.4.1). Then, computing the above expectation, it results that

$$\ln f_{\mathbf{y}}(\mathbf{y}; \theta) \simeq \sigma_w^{-4} \operatorname{Re} \left(\operatorname{Tr}(\mathbf{R}^H(\theta) \widehat{\mathbf{R}}) \right) \quad (6.10)$$

where the improper sample covariance matrix,

$$\widetilde{\mathbf{R}} \triangleq \mathbf{y}\mathbf{y}^T, \quad (6.11)$$

constitutes a *sufficient statistic* for the estimation of θ_o in the studied low-SNR scenario (Section 2.4.1) and

$$\mathbf{R}(\theta) \triangleq E \left\{ \widetilde{\mathbf{R}} \right\} = e^{j2\theta} \mathbf{A}\mathbf{\Gamma}\mathbf{A}^T \triangleq e^{j2\theta} \mathbf{R}$$

stands for its expected value evaluated at θ with $\Gamma \triangleq E_{\mathbf{x}} \{\mathbf{x}\mathbf{x}^T\}$ the improper covariance matrix of the pseudo-symbols.

Notice that the quadratic form $\text{Tr}(\mathbf{R}^H \tilde{\mathbf{R}}) = \mathbf{y}^T \mathbf{R} \mathbf{y}$ is the *minimal sufficient statistic* [Kay93b] in the studied low SNR scenario. It is worth noting that it is possible to estimate the carrier phase from the second-order statistics because the pseudo-symbols \mathbf{x} do not hold the circular property [Pic94] (i.e., $\Gamma \neq \mathbf{0}$), as it happens in case of linear modulations.

Finally, the log-likelihood gradient is given by

$$\nabla(\mathbf{y}; \theta) \triangleq \frac{\partial}{\partial \theta} \ln f_{\mathbf{y}}(\mathbf{y}; \theta) = 2\sigma_w^{-4} \text{Im} \left\{ \text{Tr}(\mathbf{R}^H(\theta) \tilde{\mathbf{R}}) \right\} \quad (6.12)$$

which is in-quadrature with the likelihood function in (6.10) and vanishes for

$$\hat{\theta} = \frac{1}{2} \arg \left\{ \text{Tr}(\mathbf{R}^H \tilde{\mathbf{R}}) \right\} = \frac{1}{2} \arg \left\{ \hat{\mathbf{x}}^T \Gamma \hat{\mathbf{x}} \right\} \quad (6.13)$$

where $\hat{\mathbf{x}} \triangleq \mathbf{A}^H \mathbf{y}$ stands for the detected pseudo-symbols at the *matched filter* output [Vaz00].

The existence of an analytical solution is exceptional and an iterative algorithm is normally required to seek for the maximum of the log-likelihood function (e.g., in timing and carrier frequency synchronization [Vaz00][Men97]). Anyway, even if we have a closed-form solution (6.13), gradient-based algorithms (Section 2.5) allow the design of *closed-loop* schemes for tracking the parameter of interest in time-varying scenarios (Section 2.5). In that case, the CRB theory (Section 2.3) guarantees that the following recursion

$$\hat{\theta}_{n+1} = \hat{\theta}_n + I^{-1}(\hat{\theta}_n) \nabla(\mathbf{y}; \hat{\theta}_n) \quad (6.14)$$

attains asymptotically ($M \rightarrow \infty$) the CRB *after convergence* to the true parameter, i.e., $\hat{\theta}_n \simeq \theta_o$ [Kay93b]. Hence, the asymptotic variance of both the *open-loop* estimator in (6.13), and its *closed-loop* implementation in (6.14), is given by

$$\text{var}(\hat{\theta}) \triangleq E \left| \hat{\theta} - \theta_o \right|^2 = I^{-1} \triangleq \text{CRB} \quad (6.15)$$

where

$$I \triangleq -E \left\{ \left. \frac{\partial}{\partial \theta} \nabla(\mathbf{y}; \theta) \right|_{\theta=\theta_o} \right\} = E \{ \nabla^2(\mathbf{y}; \theta_o) \} = 4\sigma_w^{-4} \text{Tr}(\mathbf{R}^H \mathbf{R}) \quad (6.16)$$

stands for the Fisher's information [Kay93b] at low SNR, that is found to be independent of θ_o . Notice that the second-order derivative computed in (6.16) normalizes the scoring algorithm in (6.14) to yield unbiased estimates in the small-error regime ($\hat{\theta}_n \simeq \theta_o$).

Remark: equation (6.15) predicts the variance of the open-loop estimator in (6.13) *if and only if* the asymptotic (or small-error) condition holds true and, thus, (6.13) works in the linear region of the $\arg\{\cdot\}$ function. Otherwise, (6.13) becomes biased and the CRB theory fails. For instance, at low SNR, the CRB is proportional to σ_w^4 (6.15) whereas the variance of (6.13) is limited to $\pi^2/12$ bearing in mind that $|\hat{\theta}| < \pi/2$ (Fig. 6.13). Nonetheless, the small-error assumption always applies at high SNR even for short samples.

6.2.3 High-SNR Analysis: Self-noise

The main drawback of the low-SNR approximation is that it usually suffers from *self-noise* at high SNR when the sample is finite [Vaz00]. The reason is that the pseudo-pulses of the Laurent's expansion are not ISI-free, that is, $\mathbf{A}^H \mathbf{A} \neq \mathbf{I}_K$, even in case of full-response CPM formats such as MSK. Consequently, the variance of (6.13) presents a high-SNR floor. In this section, this floor is characterized and, afterwards, second-order *self-noise free* phase synchronizers are designed in Section 6.2.4.

First of all, let us compute the asymptotic variance of (6.13) for an arbitrary value of the SNR. This is done evaluating the variance of (6.14) in the steady-state ($\hat{\theta}_n \simeq \theta_0$) obtaining, after some tedious manipulations (Appendix 6.A), that

$$\text{var}(\hat{\theta}) = I^{-2} E\{\nabla^2(\mathbf{y}; \theta_0)\} = 2\sigma^{-8} I^{-2} \mathbf{r}^H \mathbf{Q} \mathbf{r} = \frac{\mathbf{r}^H \mathbf{Q} \mathbf{r}}{8 \text{Tr}^2(\mathbf{R}^H \mathbf{R})} \quad (6.17)$$

where $\mathbf{r} \triangleq \text{vec}(\mathbf{R})$ stands for the column-wise stacking of \mathbf{R} , and \mathbf{Q} is the fourth-order moments matrix given by

$$\mathbf{Q} = 2\bar{\mathbf{R}} \otimes \bar{\mathbf{R}} + \mathbf{A} \mathbf{K} \mathbf{A}^T, \quad (6.18)$$

that extends the formulation in Chapter 3 to noncircular constellations with the following set of definitions:²

$$\begin{aligned} \bar{\mathbf{R}} &\triangleq E\{\mathbf{y}\mathbf{y}^H\} = \mathbf{A}\mathbf{A}^H + \sigma_w^2 \mathbf{I}_M \\ \mathbf{A} &\triangleq \mathbf{A} \otimes \mathbf{A} \\ \mathbf{K} &\triangleq \tilde{\Gamma} - 2\mathcal{P} \\ \mathcal{P} &\triangleq \frac{1}{2}(\mathbf{I}_{K^2} + \mathcal{K}) \\ \tilde{\Gamma} &\triangleq E_{\mathbf{x}}\{\text{vec}(\mathbf{x}\mathbf{x}^T) \text{vec}^H(\mathbf{x}\mathbf{x}^T)\} - E_{\mathbf{x}}\{\text{vec}(\mathbf{x}\mathbf{x}^T) \text{vec}^T(\mathbf{x}\mathbf{x}^T)\} \end{aligned} \quad (6.19)$$

where \mathcal{K} is the commutation matrix that is implicitly defined as the matrix holding that $\text{vec}(\mathbf{X}^T) = \mathcal{K} \text{vec}(\mathbf{X})$ for any matrix \mathbf{X} [Mag98, Sec. 3.7]. Likewise, \mathcal{P} is the orthogonal projector onto the subspace that contains the vectorization of *any* symmetric matrix, i.e., $\text{vec}(\mathbf{X})$ with $\mathbf{X} = \mathbf{X}^T$ [Mag98, Sec. 3.7]. It can be shown that both \mathbf{r} and $\tilde{\Gamma}$ lie in this subspace. The matrix $\tilde{\Gamma}$ is specific of the actual CPM format and can be calculated numerically. In case of MSK-type modulations, this task is simplified because $[\tilde{\Gamma}]_{i,j} \in \{0, \pm 2\}$.

Therefore, if (6.17) is evaluated in the noiseless case, one finds that the self-noise variance causing the high-SNR floor is equal to

$$\lim_{\sigma_w^2 \rightarrow 0} \text{var}(\hat{\theta}) = \frac{\mathbf{r}^H \tilde{\mathbf{A}} \tilde{\Gamma} \mathbf{A}^H \mathbf{r}}{8 \text{Tr}^2(\mathbf{R}^H \mathbf{R})}. \quad (6.20)$$

²The reader is warned that some notation is slightly redefined in this section. For example, $\mathbf{R}(\theta)$ is the *improper* covariance matrix; the conjugation is omitted in \mathbf{A} ; matrix \mathbf{K} is redefined in (6.19); and, finally, \mathbf{Q} is the covariance matrix of the new sufficient statistic $\text{vec}(\tilde{\mathbf{R}})$ (6.11)

As stated before, the estimator would be self-noise free in the absence of ISI ($\mathbf{A}^H \mathbf{A} = \mathbf{I}_K$) because in that case $\mathcal{A}^H \mathbf{r} = \text{vec}(\Gamma)$ and, thus, the term $\tilde{\Gamma} \text{vec}(\Gamma)$ in (6.20) becomes equal to zero for most noncircular modulations of interest, e.g., real-valued constellations, MSK-type signals as well as the offset QPSK format. Anyway, the estimator is consistent for *any* SNR since the self-noise variance in (6.20) turns out to be proportional to M^{-1} for $M \gg 1$. For example, the simulations in [Men97, Sec. 6.6.2] show that the variance curvature is practically inappreciable below SNR=20dB with $M = 100$ for the MSK and GMSK modulations.

6.2.4 Second-Order Optimal Estimation

The aim of this section is to deduce optimal second-order synchronization techniques for the whole SNR range. Assuming the noise variance is known (or accurately estimated), the proposed estimator will minimize the joint contribution of thermal and pattern noise, leading to the previous ML solution (6.13) when the SNR is sufficiently low and to self-noise free schemes at high SNR (Section 6.2.5).

With this purpose, let us introduce the equation of a generic second-order gradient following the structure provided by (6.12) under the low-SNR assumption:

$$\Delta(\mathbf{y}; \theta) \triangleq 2 \text{Im} \left\{ e^{-j2\theta} \text{Tr}(\mathbf{M}^H \tilde{\mathbf{R}}) \right\} = 2 \text{Im} \left\{ e^{-j2\theta} \mathbf{m}^H \tilde{\mathbf{r}} \right\} \quad (6.21)$$

where \mathbf{M} is the matrix of coefficients that should be optimized, $\mathbf{m} \triangleq \text{vec}(\mathbf{M})$ its vectorization and $\tilde{\mathbf{r}} \triangleq \text{vec}(\tilde{\mathbf{R}})$ the vectorization of (6.11).

The value of θ for which (6.21) is null is given by

$$\hat{\theta} = \frac{1}{2} \arg \left\{ \text{Tr}(\mathbf{M}^H \tilde{\mathbf{R}}) \right\} = \frac{1}{2} \arg \left\{ \mathbf{m}^H \tilde{\mathbf{r}} \right\} \quad (6.22)$$

provided that $\mathbf{m}^H \tilde{\mathbf{r}} \neq 0$. Otherwise, the open-loop algorithm in (6.22) is unable to extract any phase information from this specific $\tilde{\mathbf{r}}$. This fact will be studied in detail in Section 6.2.5 because it is *only* relevant at high SNR. For the moment, (6.22) is assumed to be “well-conditioned”.

Another important remark is that the estimation problem at hand allows obtaining a closed-form solution for the zero of $\Delta(\mathbf{y}; \theta)$. However, notice that the *open-loop* estimator proposed in (6.22) is not quadratic in the data due to the $\arg \{ \cdot \}$ operator. Therefore, the estimation techniques studied in this section should be seen as a nonlinear transformation of the sample covariance matrix $\tilde{\mathbf{R}} = \mathbf{y} \mathbf{y}^T$, that is only a sufficient statistic under the low-SNR approximation.

Thus, the variance of (6.22) in the small-error regime is given by

$$\text{var}(\hat{\theta}) = J^{-2} E \{ \Delta^2(\mathbf{y}; \theta_0) \} = 2J^{-2} \mathbf{m}^H \mathcal{P} \mathbf{Q} \mathbf{m}, \quad (6.23)$$

that can be seen as a generalization of (6.17) with J defined as the gradient slope at θ_o , that is:

$$J \triangleq -E \left\{ \frac{\partial}{\partial \theta} \Delta(\mathbf{y}; \theta) \Big|_{\theta=\theta_o} \right\} = 4 \operatorname{Re}(\mathbf{m}^H \mathbf{r}). \quad (6.24)$$

Notice that J plays the same role than the Fisher's information in (6.14)-(6.16), that is, it normalizes the recursion in (6.14) to yield unbiased estimates around the true parameter θ_o .

The optimal coefficients are obtained minimizing the estimator variance (6.23) subject to the above bias constraint (6.24). This optimization leads to an underdetermined system of equations and

$$\mathbf{m} = \frac{J \mathbf{Q}^{-1} \mathbf{r}}{4 \mathbf{r}^H \mathbf{Q}^{-1} \mathbf{r}} \quad (6.25)$$

is found to be the minimum-norm solution. Anyway, all the solutions are found to yield the same variance, that is equal to

$$\operatorname{var}(\hat{\theta}) = J^{-1} = \frac{1}{8 \mathbf{r}^H \mathbf{Q}^{-1} \mathbf{r}} \quad (6.26)$$

plugging (6.25) into (6.23). Eventually, the coefficients of the optimal estimator are given by

$$\mathbf{m} = 2 \mathbf{Q}^{-1} \mathbf{r}.$$

Finally, note that all the above expressions reduce to the ones obtained in Section 6.2.2 under the low-SNR assumption ($\sigma_w^2 \rightarrow \infty$) taking into account that

$$\mathbf{Q}^{-1} = \frac{1}{2} \sigma_w^{-4} \mathbf{I}_{M^2} + o(\sigma_w^{-4}) \quad (6.27)$$

where $o(\sigma_w^{-4})$ gathers all the terms converging to zero faster than σ_w^{-4} .

Notice that the GML estimator has not been considered in the carrier phase estimation problem because the Gaussian assumption also implies the circularity of the nuisance parameters.

6.2.5 High SNR Study: Self-noise

This section is concerned with the high-SNR study of the optimal second-order synchronizer deduced in the last section. Although the analysis is more involved than in Section 6.2.3, closed-form expressions have been obtained concluding that self-noise can be totally removed. Nonetheless, in the case of partial-response schemes (e.g., GMSK) the open-loop implementation (6.22) *may fail* when $\mathbf{m}^H \tilde{\mathbf{r}} = \mathbf{m}^H \mathcal{A} \operatorname{vec}(\mathbf{x} \mathbf{x}^T) = 0$ in the noiseless case. When this happens, the carrier phase is not identifiable from this particular observation $\tilde{\mathbf{r}}$. The reason for this abnormal behavior is that it is not always possible to cancel out the imaginary part of the argument (self-noise) while the real part is kept positive (6.22). For example, when the binary data symbols

are alternate, i.e., $\{+1, -1, +1, \dots\}$, the 2REC modulation exhibits a constant phase equal to $\pm\pi/4$ and, thus, $\tilde{\mathbf{r}} = \mathcal{A} \text{vec}(\mathbf{x}\mathbf{x}^T)$ is strictly imaginary in the noiseless case.

A deeper analysis shows that this limitation is a consequence of the singularity of matrix \mathbf{A} for partial-response modulations. However, this conclusion needs to be clarified; the singularity of \mathbf{A} is due to the *partial* contribution from the pseudo-symbols outside the observation window in the studied SCPC system (Section 6.1.2). Therefore, only in the asymptotic case ($M \rightarrow \infty$), this “border effect” is negligible and matrix \mathbf{A} is *effectively* full-rank.

The asymptotic study of (6.26) involves the computation of \mathbf{Q}^{-1} when the noise power tends to zero. Because the noiseless component of \mathbf{Q} is singular (6.19), we must resort to the inversion lemma obtaining that

$$\mathbf{m} = 2\mathbf{Q}^{-1}\mathbf{r} = \mathcal{R}^{-1}(\mathbf{I} - \mathbf{V}(2\Sigma^{-1} + \mathbf{V}^H\mathcal{R}^{-1}\mathbf{V})^{-1}\mathbf{V}^H\mathcal{R}^{-1})\mathbf{r} \quad (6.28)$$

where $\mathcal{R} \triangleq \overline{\mathbf{R}} \otimes \overline{\mathbf{R}}$ and $\mathbf{V}\Sigma\mathbf{V}^H$ is the “economy-size” diagonalization of $\mathcal{A}\mathbf{K}\mathcal{A}^H$ (6.19), i.e., Σ *only* contains the non-zero eigenvalues and, \mathbf{V} the associated eigenvectors.

Using again the inversion lemma, the high-SNR asymptotic value of $\overline{\mathbf{R}}^{-1}$ can be expanded in terms of σ_w^2 , yielding

$$\overline{\mathbf{R}}^{-1} = \sigma_w^{-2}\mathbf{P}_{\mathbf{A}}^{\perp} + \mathbf{B} - \sigma_w^2\mathbf{B}^2 + O(\sigma_w^4) \quad (6.29)$$

where $O(\sigma_w^4)$ contain all the terms converging to zero as σ_w^4 or faster, $\mathbf{P}_{\mathbf{A}}^{\perp} \triangleq \mathbf{I} - \mathbf{A}\mathbf{A}^{\#}$ stands for the orthogonal projector onto the span of matrix \mathbf{A} and

$$\mathbf{B} \triangleq (\mathbf{A}\mathbf{A}^H)^{\#}$$

is introduced to compact further equations. Thus, the limit of \mathcal{R}^{-1} is straightforward from (6.29), using that

$$\mathcal{R}^{-1} = \overline{\mathbf{R}}^{-1} \otimes \overline{\mathbf{R}}^{-1}. \quad (6.30)$$

However, all the terms in (6.30) containing $\mathbf{P}_{\mathbf{A}}^{\perp}$ go to zero when multiplied by \mathbf{V} or \mathbf{r} in (6.28) since $\text{span}\{\mathbf{V}\} \subset \text{span}\{\mathcal{A}\}$ and $\mathbf{r} = \mathcal{A} \text{vec}(\Gamma) \in \text{span}\{\mathcal{A}\}$. Therefore, considering only the surviving terms, it is found that

$$\mathcal{R}^{-1} = \mathcal{B} - \sigma_w^2(\mathbf{B} \otimes \mathbf{B}^2 + \mathbf{B}^2 \otimes \mathbf{B}) + O(\sigma_w^2) \quad (6.31)$$

for $\sigma_w^2 \rightarrow 0$ where $\mathcal{B} \triangleq \mathbf{B} \otimes \mathbf{B} = (\mathcal{A}\mathcal{A}^H)^{\#}$.

To complete the deduction, the inversion lemma has to be used once again in order to compute the inner inverse in (6.28) because

$$\mathbf{T} \triangleq 2\Sigma^{-1} + \mathbf{V}^H\mathcal{B}\mathbf{V}$$

turns out to be singular again. Precisely because of that, the second term of (6.28) becomes proportional to σ_w^{-2} and prevails at high SNR avoiding the variance floor. Taking this fact into account, the high-SNR asymptotic expression of \mathbf{m} is given by

$$\mathbf{m} = \sigma_w^{-2} \mathbf{B} \mathbf{V} \mathbf{P}_T^\perp \mathbf{V}^H \mathbf{B} \mathbf{r} + O(1) \quad (6.32)$$

with

$$\begin{aligned} \mathbf{P}_T^\perp &\triangleq \mathbf{U}^{-1} (\mathbf{I} - \mathbf{V}_T (\mathbf{V}_T^H \mathbf{U}^{-1} \mathbf{V}_T)^{-1} \mathbf{V}_T^H \mathbf{U}^{-1}) \\ \mathbf{U} &\triangleq \mathbf{V}^H (\mathbf{B} \otimes \mathbf{B}^2 + \mathbf{B}^2 \otimes \mathbf{B}) \mathbf{V} \end{aligned} \quad (6.33)$$

The above expression is general no matter if \mathbf{A} is singular or not. In case \mathbf{A} is full-rank, (6.32) can be simplified if the deduction is started again by decomposing the first term of \mathbf{Q} as $\mathcal{A} \mathbf{V}_K \Sigma_K \mathbf{V}_K^H \mathcal{A}^H$ with Σ_K the diagonal matrix having the non-zero eigenvalues of \mathbf{K} and \mathbf{V}_K the related eigenvectors. Thus, if \mathbf{V} and Σ are redefined as $\mathbf{V} = \mathcal{A} \mathbf{V}_K$ and $\Sigma = \Sigma_K$, respectively, (6.32) can be written as follows:

$$\mathbf{m} = \sigma_w^{-2} \mathcal{A}^{\#H} \mathbf{V}_K \mathbf{P}_T^\perp \mathbf{V}_K^H \mathcal{A}^{\#} \mathbf{r} + O(1) \quad (6.34)$$

using that $\mathcal{A}^H \mathbf{B} = \mathcal{A}^{\#}$ and $\mathbf{T} = 2\Sigma_K^{-1} + \mathbf{I}$.

At this point, it is worth understanding that the obtained solution differs from the standard CML estimator (Section 2.4.2) in that (6.34) *cannot* project the self-noise term onto the orthogonal subspace of \mathbf{A} because they are collinear [Vaz00][Rib01b]. Alternatively, in (6.34) the received signal \mathbf{y} is passed through a *zero-forcing* equalizer $\mathbf{A}^{\#}$ in order to decorrelate the received pseudo-symbols [Vaz00] and, afterwards, the outer product of the detected pseudo-symbols is projected onto the matrix $\mathbf{V}_K \mathbf{P}_T^\perp \mathbf{V}_K^H$ whose span *coincide with* that of $\mathbf{P}_{\tilde{\Gamma}}^\perp$, which is the orthogonal projector onto the subspace generated by $\tilde{\Gamma}$ (6.19). The key property of $\mathbf{P}_{\tilde{\Gamma}}^\perp$ —inherited by $\mathbf{V}_K \mathbf{P}_T^\perp \mathbf{V}_K^H$ —is that $\mathbf{P}_{\tilde{\Gamma}}^\perp \text{vec}(\mathbf{x}\mathbf{x}^T)$ is real-valued for any possible vector \mathbf{x} .

Resuming the initial discussion, if \mathbf{A} is full-rank, the zero-forcer recovers without error the vector of pseudo-symbols, i.e., $\hat{\mathbf{x}} = \mathbf{A}^{\#} \mathbf{y} = \mathbf{x}$ and $\mathbf{V}_K \mathbf{P}_T^\perp \mathbf{V}_K^H$ is able to eliminate the imaginary part of $\text{vec}(\mathbf{x}\mathbf{x}^T)$ that causes the referred self-noise while the real part is preserved, allowing feed-forward estimation (6.22). Otherwise, the real and imaginary parts are coupled and the self-noise cancellation attenuates inevitably the real part too.

To conclude this section, the estimator variance at high SNR is given by

$$\text{var}(\hat{\theta}) = \frac{\sigma_w^2}{4 \text{vec}^H(\Gamma) \mathcal{A}^{\#} \mathbf{V} \mathbf{P}_T^\perp \mathbf{V}^H \mathcal{A}^{\#H} \text{vec}(\Gamma)} + o(\sigma_w^2) \quad (6.35)$$

for the general case (6.32) and, reduces to

$$\text{var}(\hat{\theta}) = \frac{\sigma_w^2}{4 \text{vec}^H(\Gamma) \mathbf{V}_K \mathbf{P}_T^\perp \mathbf{V}_K^H \text{vec}(\Gamma)} + o(\sigma_w^2) \quad (6.36)$$

when \mathbf{A} is full-rank (6.34). Notice that in both cases the estimators are consistent, i.e., the denominator increases without limit as M is augmented.

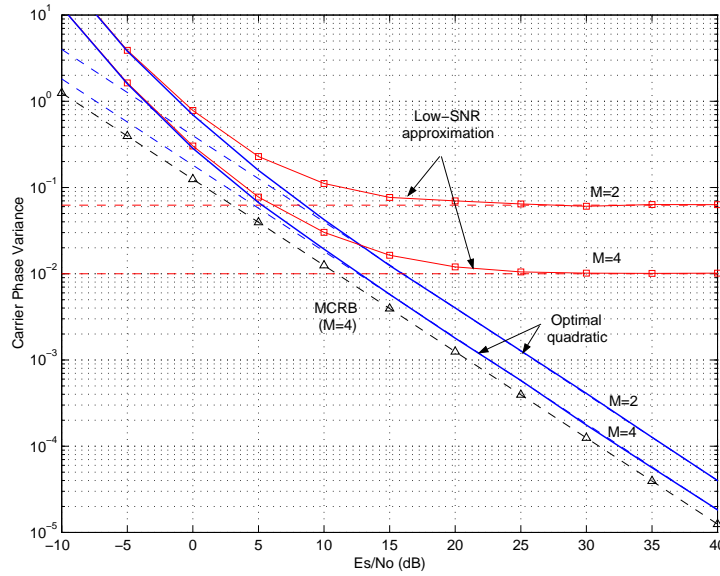


Figure 6.13: Carrier phase variance as a function of the SNR for the MSK modulation with $N_{ss} = 2$. Dotted lines correspond to the high-SNR bounds computed in Sections 6.2.3 and 6.2.5.

6.2.6 Numerical Results

This section validates via simulation the theoretical results presented in this case study. The steady-state variance of the *closed-loop* solution presented in equation (6.14) is evaluated for both the low-SNR approximation and the optimal second-order synchronizer deduced in Section 6.2.4 (see Fig. 6.13 and Fig. 6.14). Simulations show that the proposed solution is self-noise free even if the observation is rather short ($M = 2, 4$). Furthermore, the high-SNR asymptotic expressions obtained in (6.20), (6.35) and (6.36) exhibit a perfect match at high SNR. Although it is not plotted, the feedforward synchronizer derived in (6.22) was tested for the MSK modulation in Fig. 6.13 confirming that it is *always* self-noise free.

Surprisingly, the high-SNR estimators deduced in (6.32) and (6.34) are also exact for any SNR. The reason is that, as mentioned before, there is no noise-enhancement at low-SNR because (6.32) and (6.34) does not include the orthogonal projector $\mathbf{P}_{\mathbf{A}}^\perp$.

Finally, the acquisition performance of the optimal closed-loop synchronizer is evaluated in Fig. 6.15 in order to validate its operability when \mathbf{A} is singular in case of partial-response schemes (e.g., 3REC). In the same figure, the probability of “failure” has been computed as a function of the observation length for some partial response schemes. As shown in the plot, the probability of failure decays exponentially with the observation time and the damping factor increases if the modulator memory is shortened.

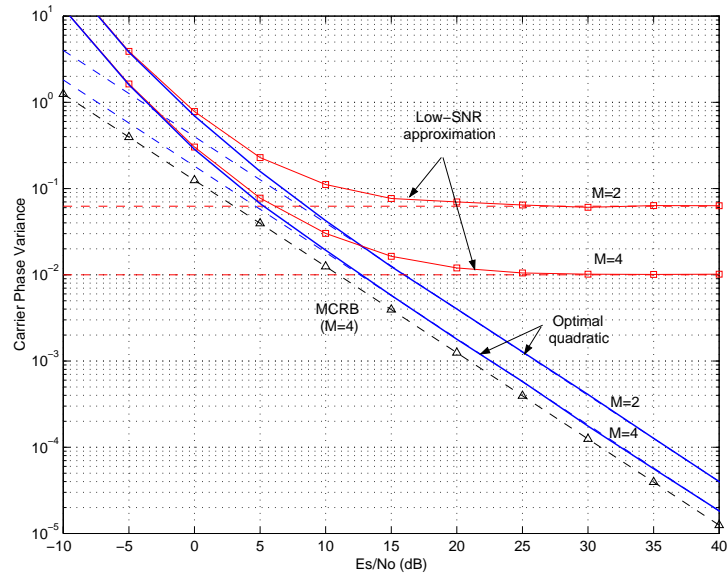


Figure 6.14: Carrier phase variance as a function of the SNR for the 3REC modulation with $N_{ss} = 4$.

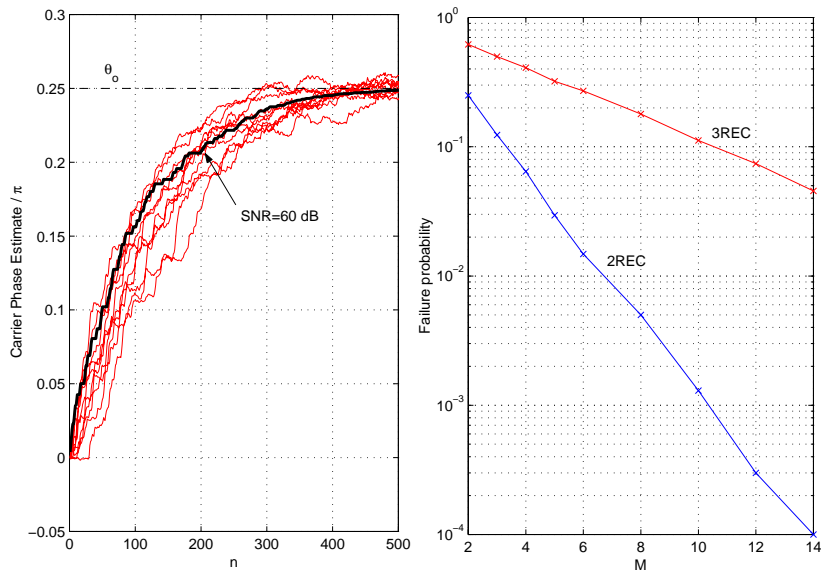


Figure 6.15: On the left side, 10 acquisitions for the 3REC modulation with $N_{ss} = 2$ and $M = 2$. The SNR was set to 20 dB and the loop step-size fixed to $\mu = 0.01$. On the right-hand side, the probability of failure for 2REC and 3REC with $N_{ss} = 2$ and $\sigma_w^2 = 0$.

6.3 TOA Estimation in Multipath Scenarios

In the context of wireless, underwater or optical communications, the transmitted signal is severely distorted by the channel due to the so-called multipath propagation. In a multipath scenario, the received signal is the sum of multiple replicas of the transmitted waveform whose delays, amplitudes and phases are unknown. The resulting dispersive channel can be modeled as a finite impulse response (FIR) filter of unknown complex-valued coefficients. In digital communications, the multipath disturbance is mitigated implementing digital equalizers in order to prevent intersymbol interference (ISI). This topic is addressed in Section 6.4 where blind channel estimators are designed from the sample covariance matrix.

In this section, we focus on the problem of radiolocation in cellular networks using range estimates from several base stations. Range information can be obtained estimating the time of arrival (TOA) –if the network is synchronous– or the time difference of arrival (TDOA) in case of an asynchronous cellular network. Although the principle is the same than in radar and navigation applications (e.g., GPS or GALILEO), the mobile radio channel poses some additional impairments as, for example, time- and frequency-selective fast fading, non line-of-sight (NLOS) conditions, narrowband signaling in case of second generation terminals, low E_s/N_0 for the received signal coming from the non-serving base stations, limited training periods for TOA estimation (e.g., GSM midamble), etc.

In this context, a lot of effort has been made to design TOA estimators robust to the multipath degradation. Some of them have been developed for satellite positioning systems (i.e., GPS, GLONASS and, GALILEO) using direct sequence spread spectrum signaling, e.g., [Bra01][Sec00, Sec. 2.2.2.] and references therein. All these contributions are intended for single-antenna receivers. Nonetheless, it has been proved that the use of antenna arrays is useful to mitigate multipath and also to cancel interferences [Sec00]. Actually, a multisensor receiver is able to combine direction of arrival (DOA) and TOA information in order to render more accurate position estimates.

The application of these techniques to third generation cellular systems such as UMTS is rather straightforward since they share the same signal format. On the other hand, timing recovery in narrowband systems (e.g., GSM) becomes more difficult since the time resolution is inversely proportional to the signal bandwidth and, the self-noise contribution becomes critical for the working SNRs. Recall that self-noise consists of the intersymbol interference (ISI) at the timing error detector output. In spread spectrum communications, the self-noise term is negligible because it is filtered out in the despreading stage.

Some relevant contributions in the context of narrowband communications are [Chi94][Mog03] and, [Fis98][Win00][Rib02]. In the first two proposals, the Gaussian assumption is adopted and non-data-aided TOA estimators are deduced. On the other hand, the last

three papers rely on the transmission of known training data. In all the papers, with the exception of [Rib02], the channel coefficients are deterministic unknowns that need to be estimated in a first step. An alternative approach is adopted in [Rib02] where the multipath is modeled as a random term of known first- and second-order moments. In this manner, unbiased TOA estimates are obtained trading some estimation variance following a Bayesian approach.

In this section, the problem of both DA and NDA timing –and also carrier frequency–offset–estimation is studied in a multipath scenario assuming that the channel response is unknown. Optimal second-order *unbiased* estimators are deduced based on the channel first- and second-order statistics following a similar approach to the one presented in [Rib02]. Some numerical results are presented for the problem of TOA estimation in a typical wireless outdoor scenario in the context of the GSM standard and the EMILY European project [Bou02a][Bou02b].

The results in this section were partially presented in the the International Zurich Seminar on Broadband Communications that was held in Zurich in 2002 [Vil02a]:

- “Optimal Quadratic Non-Assisted Parameter Estimation for Digital Synchronisation”. J. Villares, G. Vázquez. Proceedings of the *International Zurich Seminar on Broadband Communications 2002* (IZS2002). pp. 46.1-46.4. Zurich (Switzerland). February 2002.

6.3.1 Signal Model

Let us consider that the channel impulse response is time-invariant during the observation time (M samples). The channel low-pass equivalent impulse response *within the receiver bandwidth* W is given by

$$h(t) = \frac{1}{W} \sum_{k=0}^{L-1} h(k/W) \operatorname{sinc}(Wt - k) \quad (6.37)$$

with L/W the effective duration of the channel [Pro95, Sec. 5-1, Ch. 14]. Hereafter, the bandwidth W is set to $2/T$ (100% excess of bandwidth) in order to admit the majority of bandpass modulations.

The channel taps $h(k/W)$ will be modeled as *zero-mean* complex Gaussian variables with their envelope and phase following a Rayleigh and uniform distribution, respectively. The Rayleigh distribution is adopted hereafter because it corresponds to a worst-case situation. Anyway, it is possible to assume for the first coefficient of $h(k/W)$ a Rician distribution in order to take into account the line-of-sight (LOS) component [Gre92].

From the above considerations, the complex envelope of the received signal at the sampler

output can be written as

$$y(mT_s) = \sum_{i=-\infty}^{\infty} d_i \sum_{k=0}^{L-1} h(k/W) e^{j2\pi\nu m/N_{ss}} p(mT_s - k/W - iT - \tau T) + w(mT_s) \quad (6.38)$$

where T_s is the sampling period, $\{d_i\}$ is the sequence of transmitted symbols, ν and τ are the frequency and timing errors normalized with respect to the symbol time $T = N_{ss}T_s$, $p(t)$ is the shaping pulse, and $w(t)$ the stationary AWGN term. Following the guidelines in Section 6.1.2, the above formula can be expressed in vectorial form as follows:

$$\mathbf{y} = \mathbf{A}(\lambda) \mathbf{H} \mathbf{d} + \mathbf{w} = \mathbf{A}(\lambda) \mathbf{x} + \mathbf{w} \quad (6.39)$$

where λ stands for either the timing or frequency error and the columns of \mathbf{H} are $1/W$ -seconds delayed versions of the channel impulse response $h(k/W)$. It is really important to realize that the inclusion of a random channel $h(t)$ yields directly the same model in (6.3), except that the proposed estimators will have to cope with the extended, correlated vector of symbols

$$\mathbf{x} \triangleq \mathbf{H} \mathbf{d}.$$

Therefore, the channel has two negative effects:

1. Firstly, the unknown vector of symbols \mathbf{x} is about WT times longer than the vector of transmitted symbols \mathbf{d} . The increment of the nuisance parameters will establish a limit on the variance of blind estimators when dealing with a time dispersive channel.
2. Secondly, the channel modifies the covariance of the transmitted symbols in the following way:

$$\Gamma \triangleq E \{ \mathbf{x} \mathbf{x}^H \} = E_{\mathbf{H}} \{ \mathbf{H} \mathbf{H}^H \}$$

assuming again uncorrelated symbols.

Notice that the Gaussian assumption is verified in case of constant amplitude modulations such as MPSK or CPM. On the other hand, the received symbols are not strictly Gaussian when the transmitted signal is a multilevel modulation such as QAM or APK. However, it can be shown that in that case the Gaussian assumption yields practically optimal second-order estimators for any SNR.

6.3.2 Optimal Second-Order NDA Estimator

The optimal second-order estimator of λ from the above signal model is deduced in the following lines. First, the covariance matrix $\mathbf{R}(\lambda)$ and the fourth-order matrix $\mathbf{Q}(\lambda)$ are calculated, having

that

$$\begin{aligned}\mathbf{R}(\lambda) &= \mathbf{A}(\lambda) \Gamma \mathbf{A}^H(\lambda) + \mathbf{R}_w \\ \mathbf{Q}(\lambda) &= \mathbf{R}^*(\lambda) \otimes \mathbf{R}(\lambda) + \mathcal{A}(\lambda) \mathbf{K} \mathcal{A}^H(\lambda)\end{aligned}\quad (6.40)$$

where the kurtosis matrix \mathbf{K} is *diagonal* in the presence of multipath because $\mathbf{x} = \mathbf{H}\mathbf{d}$ is always circular even if the transmitted symbols \mathbf{d} are not. Moreover, \mathbf{K} is strictly zero for any constant amplitude modulation and admits a simple form in case of a linear *circular* modulation. Taking into account that

$$\mathbf{K} = E_{\mathbf{d}}\{\text{vec}(\mathbf{d}\mathbf{d}^H) \text{vec}^H(\mathbf{d}\mathbf{d}^H)\} - \text{vec}(\mathbf{I}) \text{vec}^H(\mathbf{I}) - \mathbf{I}$$

is equal to

$$\mathbf{K} = (\rho - 2) \text{diag}(\text{vec}(\mathbf{I}))$$

in case of circular constellations (3.12), it follows that the diagonal entries of \mathbf{K} are

$$[\mathbf{K}]_{k,k} = 2(\rho - 1) \sum_{i=-\infty}^{\infty} PDP^2(k/W - iT) \quad (6.41)$$

where

$$PDP(t) \triangleq \begin{cases} E\{|h(t)|^2\} & 0 \leq t < L/W \\ 0 & \text{otherwise} \end{cases}$$

stands for the channel power delay profile (PDP). Notice that (6.41) vanishes in case of constant amplitude modulations ($\rho = 1$). Thus, the Gaussian assumption in a multipath scenario applies for an important class of modulations whereas it is not verified in case of Gaussian distributed symbols ($\rho = 2$).

In some circumstances, the channel taps are uncorrelated and, if WT is an integer number, Γ is a diagonal matrix with entries:

$$[\Gamma]_{k,k} = \sum_{i=-\infty}^{\infty} PDP(k/W - iT)$$

In this uncorrelated scattering (US) scenario, the channel PDP conveys all the statistical information about the channel. Then, assuming that the channel PDP is known or accurately estimated, optimal second-order synchronizers can be built for the studied scenario using the framework provided in Chapter 3 and 4.

Moreover, in some situations a limited set of parameters is sufficient to describe completely the *PDP* function. For example, sometimes the mobile radio channel is correctly modeled by adopting a (decreasing) exponential *PDP* [Gre92] as the following:

$$PDP(t; \sigma) = C \exp\left(\frac{-t}{\sigma}\right) \quad (6.42)$$

where σ is the so-called delay spread and C is a normalization constant forcing $\text{Tr}\{\Gamma\} = K$ with K the length of \mathbf{x} .

Depending on the channel delay spread, two asymptotic situations can be studied:

1. Flat fading channel ($\sigma \rightarrow 0$):

$$[\Gamma]_{k,k} = \begin{cases} 1 & k \text{ multiple of } WT \\ 0 & \text{otherwise} \end{cases} \quad (6.43)$$

and hence (6.39) reduces to the ideal channel case with $\mathbf{x} = \mathbf{d}$. In that case, the channel only changes the distribution of the received symbols.

2. Highly frequency-selective channel ($\sigma \rightarrow \infty$):

$$\Gamma = \frac{1}{WT} \mathbf{I}_K \quad (6.44)$$

and, therefore, the channel is implicitly increasing the vector of received symbols \mathbf{x} in (6.39) by a factor of WT , as well as changing their distribution. Notice that this expansion may require to oversample the received signal in order to guarantee that the matrix $\mathbf{A}(\lambda)$ is tall, i.e., it has more rows (received samples) than columns (unknown symbols). Otherwise, the estimator variance will exhibit a high-SNR floor because the self-noise term cannot be cancelled. This fact forces the designer to ensure that $N_{ss} > WT$.

6.3.3 Optimal Second-Order DA Estimator

Thus far, the vector of transmitted symbols \mathbf{d} is unknown at the receiver side and, therefore, NDA estimators are required. Next, the optimal DA estimator is formulated assuming that \mathbf{d} is deterministic (i.e., a training sequence) but the channel \mathbf{H} is still unknown. In that case, the received symbols $\mathbf{x} = \mathbf{H}\mathbf{d}$ are *zero-mean* random variables and, hence, second-order methods are necessary once more. In order to deduce the optimal second-order estimator, the signal model in (6.39) must be modified in the following way:

$$\mathbf{y} = \mathbf{A}(\lambda) \mathbf{D}\mathbf{h} + \mathbf{w} \quad (6.45)$$

with $[\mathbf{h}]_k = h(k/W)$ the k -th tap of the unknown channel and \mathbf{D} the matrix stacking the known transmitted symbols $\{d_i\}$ in such a way that $\mathbf{D}\mathbf{h} = \mathbf{H}\mathbf{d}$.

At this point, the optimal second-order estimator of λ is straightforward from the above signal model with \mathbf{h} the vector of Gaussian nuisance parameters. It only rests to compute the covariance matrix $\mathbf{R}(\lambda)$ and the fourth-order matrix $\mathbf{Q}(\lambda)$ for the problem at hand, obtaining that

$$\begin{aligned} \mathbf{R}(\lambda) &= \mathbf{A}(\lambda) \mathbf{D}\Gamma_h \mathbf{D}^H \mathbf{A}^H(\lambda) + \mathbf{R}_w \\ \mathbf{Q}(\lambda) &= \mathbf{R}^*(\lambda) \otimes \mathbf{R}(\lambda) \end{aligned}$$

where

$$\Gamma_h \triangleq E \{ \mathbf{h} \mathbf{h}^H \}$$

and $\mathbf{Q}(\lambda)$ is computed taking into account that \mathbf{h} is normally distributed. In case of uncorrelated scattering, Γ_h becomes diagonal with entries $[\Gamma_h]_{k,k} = PDP(k/W)$.

6.3.4 Numerical Results

The results in this section were applied to devise multipath resistant TOA estimators in the context of the EMILY project [Bou02b]. The aim of this project was the integration of positioning measurements from the GPS and GSM networks. In the second case, the spatial accuracy is severely degraded due to the multipath propagation. In this kind of scenarios the proposed NDA and DA estimators are robust against the multipath providing unbiased TOA estimates. In both cases, the channel PDP and the noise variance is measured off-line. For the sake of simplicity, an uncorrelated Rayleigh channel having exponential PDP is considered. Different delay spreads are simulated and the channel is varied in time according to the Jake's Doppler spectrum [Gre92] although this information is not exploited by the estimator. Finally, the GMSK modulation from the GSM standard as well as the MPSK and MSK modulations are considered in the simulations.

To estimate the timing error τ , the received bandpass signal is filtered into $W = 2/T$ and, afterwards, the I and Q components are generated and sampled taking $N_{ss} = 4$ per symbol. A first-order closed-loop is implemented to estimate and track the TOA of the user of interest. The optimal second-order NDA discriminator is considered with $M = 8$ the number of input samples. The variance at the discriminator output is computed as a function of the SNR. Notice that this variance is further reduced by the loop filter. Simulations fit pretty well with the theoretical performance obtained in Chapter 4, where it is shown that the minimum variance for any quadratic unbiased timing detector is given by

$$VAR(\tau) = \frac{1}{\mathbf{d}_r^H(\tau) \mathbf{Q}^{-1}(\tau) \mathbf{d}_r(\tau)} \quad (6.46)$$

with

$$\mathbf{d}_r(\tau) \triangleq \text{vec} \left(\frac{d\mathbf{R}(\tau)}{d\tau} \right) = \text{vec} \left(\mathbf{A}(\tau) \frac{d\mathbf{A}^H(\tau)}{d\tau} + \frac{d\mathbf{A}(\tau)}{d\tau} \mathbf{A}^H(\tau) \right)$$

and $d\mathbf{A}(\tau)/d\tau$ the matrix whose columns are $1/W$ -delayed versions of the shaping pulse derivative, i.e., $dp(t)/dt$. Notice that the estimator variance in (6.46) becomes independent of the actual value of the parameter τ .

The first simulation in Fig. 6.16 is carried out for the 16-QAM modulation. As commented before, the number of *significant* nuisance parameters grows with the delay spread σ . In Fig.

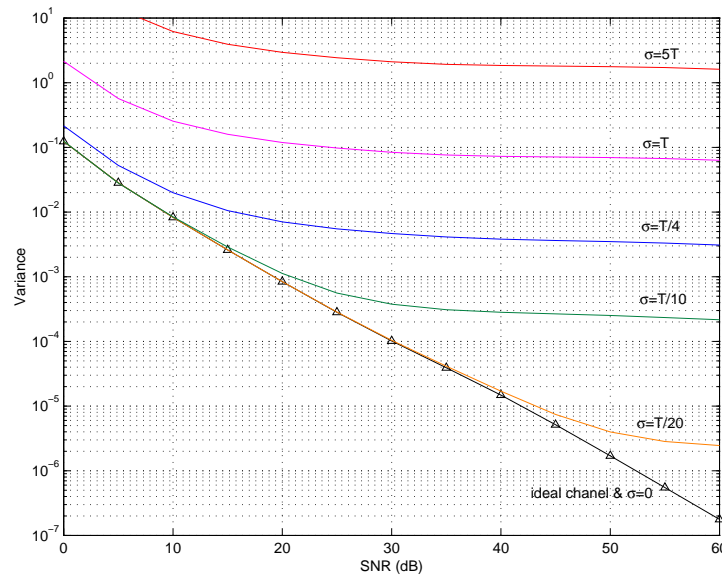


Figure 6.16: TOA estimation variance as a function of the SNR for 16-QAM symbols. The simulation parameters are $N_{ss} = 4$ and $M = 8$. The transmitted pulse is a square-root raised cosine truncated at $\pm 4T$ (100% roll-off).

6.16, the estimator is unable to cope with the self-noise enhancement and exhibits a variance floor at high SNR. This degradation is rapidly observed even for very small values of σ (e.g., $\sigma = T/10$). If σ is slightly augmented ($\sigma = T/4$), this degradation is also observed at low SNR. In the limit ($\sigma \rightarrow \infty$), the number of nuisance parameters is multiplied by $WT = 2$. Notice that the loss in terms of timing accuracy caused by the channel is extremely important in case of QAM modulated signals.

On the other hand, the maximum loss with constant modulus constellations such as MPSK, MSK and LREC is bounded and occurs when the delay spread approaches the symbol time (Figs. 6.17-6.20). The estimator is found to be self-noise free for the MPSK and MSK modulations whatever the channel delay spread. This loss is manifested first at high SNR, as it was observed in the QAM simulations (Fig. 6.16). On the other hand, self-noise can be eliminated augmenting the observation time when dealing with the 2REC and 3REC modulations.

Regarding the Gaussian assumption, it is always verified for the QAM modulation (Fig. 6.16). On the other hand, it applies for any constant modulus modulation (e.g., MPSK and CPM) in the presence of a fading channel (Figs. 6.17-6.20).

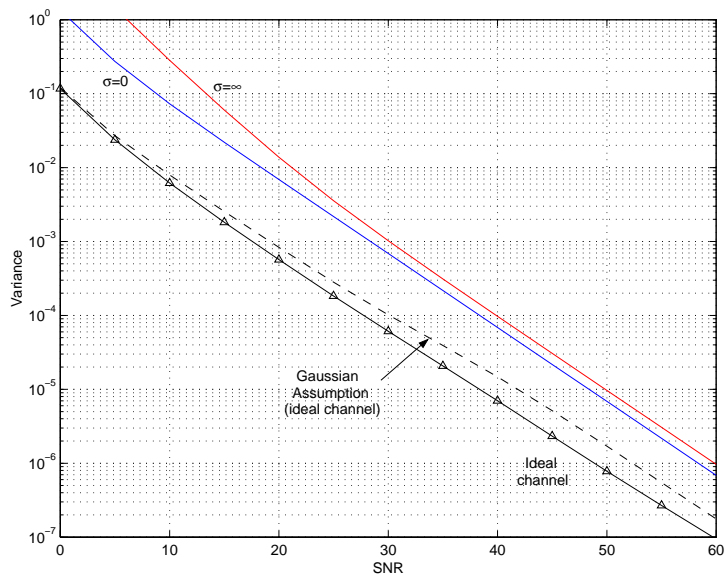


Figure 6.17: TOA estimation variance as a function of the SNR for MPSK symbols. The simulation parameters are $N_{ss} = 4$ and $M = 8$. The transmitted pulse is a square-root raised cosine truncated at $\pm 4T$ (100% roll-off).

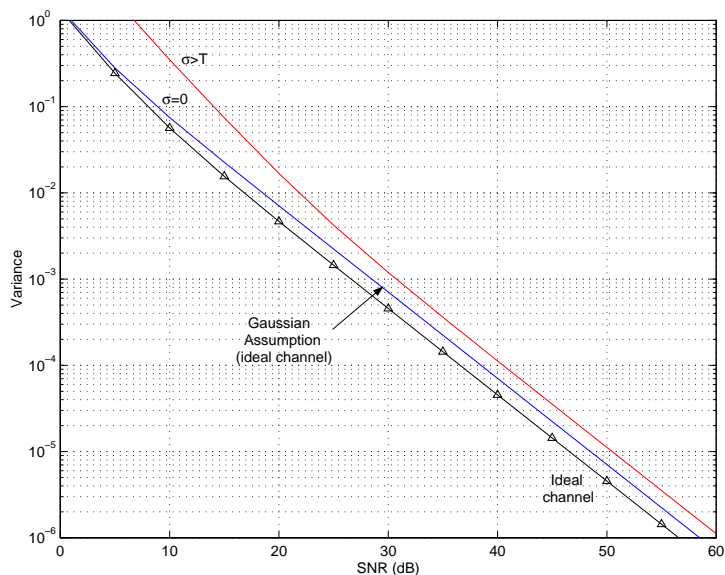


Figure 6.18: TOA estimation variance as a function of the SNR for MSK symbols. The simulation parameters are $N_{ss} = 4$ and $M = 8$.

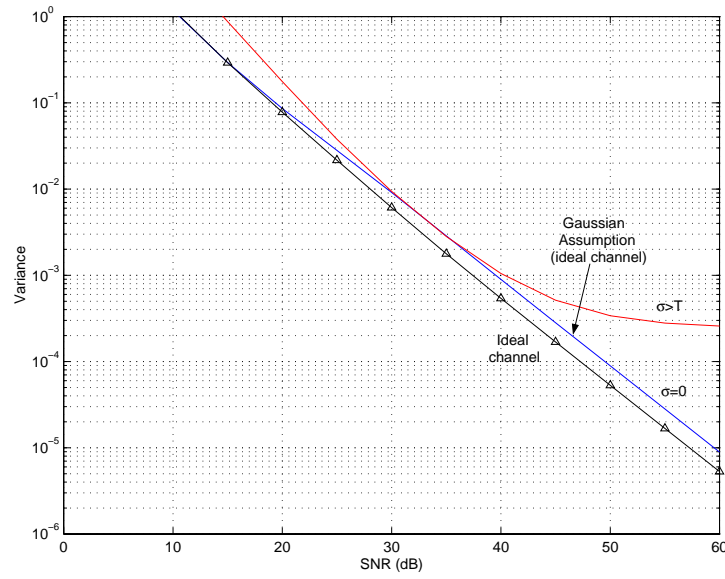


Figure 6.19: TOA estimation variance as a function of the SNR for the 2REC modulation. The simulation parameters are $N_{ss} = 4$ and $M = 8$.

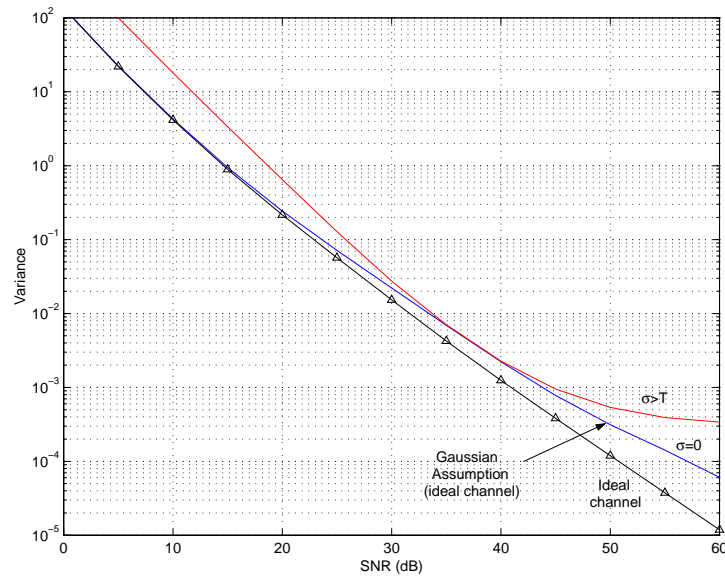


Figure 6.20: TOA estimation variance as a function of the SNR for the 3REC modulation. The simulation parameters are $N_{ss} = 4$ and $M = 8$.

6.4 Blind Channel Identification

In some scenarios, the transmission channel is frequency-selective causing intersymbol interference (ISI) at the matched filter output [Pro95]. Most times the channel response is not known a priori and the receiver has to identify the channel in order to cope with this ISI. This task is mandatory if the channel response is time-variant as it happens in wireless communications. In that case, adaptive techniques have to be developed to track the channel evolution. On the other hand, in a given access network, the subscribers have different channel responses and, thus, their equipments are supposed to configure themselves when they are plugged for the first time to the network.

In most standards, some training or pilot symbols are transmitted periodically to facilitate the receiver synchronization and the channel identification. The use of training sequences reduces the system efficiency, mostly when the channel varies in time. This inconvenience has motivated for a long time the study of blind channel estimation and equalization techniques. The pioneering work is authored by Y. Sato [Sat75] and was further developed by Godard [God80], Treichler et al. [Tre83], Benveniste et al. [Ben84], Picci et al. [Pic87], Salvi et al. [Sha90], Giannakis et al. [Gia89], Nikias [Nik92], Sala [Sal97] among others.

All these methods exploit the higher-order moments of the received signal in the belief that non-minimum phase channels were not identifiable from second-order techniques³. This idea was refuted in the revolutionary paper by Tong et al. [Ton91] where the authors proved that the channel response can be identified from the second-order moments if the received signal is cyclostationary and multiple samples per symbol are taken from the channel output. This new perspective is founded into the fractionally-spaced equalizer proposed by Ungerboeck in 1976 [Ung76]. In this paper, the oversampling was proposed as a means of improving the equalizer performance in the presence of timing errors. Anyway, the main advantage of second-order methods is that their convergence is faster than the one of higher-order methods.

The original paper was further simplified by Moulines et al. in [Mou95] and studied in [Ton94][Ton95][Tug95] from different points of view. All these channel estimators are subspace methods based on the eigendecomposition of the sample covariance matrix. A different perspective was introduced by Giannakis et al. [Gia97] and Zeng et al. [Zen97a] in which the *asymptotic (large sample)* best quadratic unbiased channel estimator is formulated from the cyclic spectrum or the cyclic correlation, respectively. Additionally, an hybrid method including subspace constraints is proposed in [Zen97a]. The resulting estimator is shown to encompass most second-order methods in the literature [Gia97][Liu93][Mou95][Sch94] [Ton95]. Some asymptotic studies are also supplied in [Zen97b].

³A system is minimum phase if all the zeros of its transfer function are inside the unit circle. This implies that the inverse system is realizable.

In this chapter, the best quadratic unbiased estimator is deduced *for a finite observation*. The proposed estimator exploits the knowledge on the pulse shaping as well as the statistics of the transmitted discrete symbols. It is found that the optimal solution is able to estimate the channel amplitude in case of constant-modulus constellations such as MPSK or CPM. On the other hand, the amplitude is ambiguous under the Gaussian assumption. This contribution actually complements the results in [Gia97][Zen97a][Zen97b].

6.4.1 Signal Model

This section is based on the signal model presented in Section 6.3.1. The aim is now to estimate the channel impulse response $h(k/W)$ in (6.37). The vector of parameters is given by

$$\boldsymbol{\theta} \triangleq [\operatorname{Re}\{h_0\}, \dots, \operatorname{Re}\{h_{L-1}\}, \operatorname{Im}\{h_0\}, \dots, \operatorname{Im}\{h_{L-1}\}]^T$$

with $h_k \triangleq h(k/W)$ the k -th tap of the channel.

The received waveform is the superposition of L replicas of the transmitted pulse $p(t)$,

$$\sum_{k=0}^{L-1} h_k p(t - k/W) \quad (6.47)$$

that, if it is sampled every $T_s = T/N_{ss}$ seconds, yields the following transfer matrix $\mathbf{A}(\boldsymbol{\theta})$:

$$\mathbf{A}(\boldsymbol{\theta}) = \sum_{k=0}^{L-1} h_k \mathbf{B}(k/W)$$

where

$$[\mathbf{B}(\tau)]_{m,i} = p(mT_s - \tau - iT) \quad m = 0, \dots, M-1, \quad i = 0, \dots, I-1$$

is the matrix performing the convolution with the delayed shaping pulse $p(t - \tau)$ and I is the number of observed symbols.

Notice that the proposed signal model can be applied in spread spectrum communications with $p(t)$ the known signature and \hat{h}_k^* the weight associated to the k -th finger in a RAKE receiver. The optimality of the RAKE receiver is guaranteed if the L fingers are uncorrelated which means that $p(t)$ is spectrally white and the channel taps h_k are uncorrelated, as well.

In the context of narrowband communications, the identification of the channel impulse response $h(k/W)$ is required to implement fractional equalizers [Ung76]. On the other hand, if the estimated channel is later employed to implement the maximum likelihood sequence estimator (MLSE) [For72][Pro95, Sec. 5-1-4] and detect the sequence of transmitted symbols without incurring in noise-enhancement, the objective is to estimate the *complex* channel response at the

matched filter output sampled at one sample per symbol, that is,

$$\alpha_n = \sum_{k=0}^{L-1} k_k g(nT - k/W) \approx \sum_{k=0}^{L-1} h_k \text{sinc}(n - k/WT)$$

where $g(t) \triangleq \int p(\tau)p(t + \tau)d\tau$ stands for the shaping pulse at the matched filter output and the last equality holds if $g(t)$ is an ideal Nyquist pulse without truncation. Although it is not strictly necessary, hereafter WT is assumed to be an integer for the sake of simplicity. In that case the vector of real parameters becomes

$$\boldsymbol{\alpha} \triangleq [\text{Re}\{\alpha_0\}, \dots, \text{Re}\{\alpha_{N-1}\}, \text{Im}\{\alpha_0\}, \dots, \text{Im}\{\alpha_{N-1}\}]^T = \mathbf{G}\boldsymbol{\theta},$$

which is a linear transformation of $\boldsymbol{\theta}$ given by matrix $\mathbf{G} \triangleq \mathbf{I}_2 \otimes \mathbf{T}$ with $N \triangleq L/WT$ and

$$[\mathbf{T}]_{n,k} \triangleq g(nT - k/W) \approx \text{sinc}(n - k/WT).$$

Taking now into account that the estimator is invariant in front of any linear transformation, the optimal second-order estimator of $\boldsymbol{\alpha}$ is directly given by $\hat{\boldsymbol{\alpha}} = \mathbf{G}\hat{\boldsymbol{\theta}}$. Therefore, if an unbiased estimator of $\boldsymbol{\alpha} = \mathbf{G}\boldsymbol{\theta}$ is aimed, it has to guarantee that $\mathbf{M}^H \mathbf{D}_r = \mathbf{I}_{2N}$ and, hence, the IPI-free solution stated in (4.12) must be adopted (see Section 4.4).

Once the signal model is identified, the procedure for deducing the optimal second-order estimator is systematic and consists in finding the set of constituent matrices in (4.12) for the problem at hand. Regarding the matrix of derivatives \mathbf{D}_r , the first coefficient h_0 is supposed to be real valued in order to solve the phase ambiguity of second-order algorithms.

Eventually, the matrix \mathbf{D}_r is built stacking the derivatives of the vectorized covariance matrix $\mathbf{r}(\boldsymbol{\theta}) = \text{vec}(\mathbf{R}(\boldsymbol{\theta}))$ with respect to the real and imaginary part of the complex coefficients h_k :

$$\begin{aligned} \partial \mathbf{r}(\boldsymbol{\theta}) / \partial \text{Re}\{h_k\} &= \text{vec}[\mathbf{B}(k/W) \mathbf{A}^H(\boldsymbol{\theta}) + \mathbf{A}(\boldsymbol{\theta}) \mathbf{B}^H(k/W)] \\ \partial \mathbf{r}(\boldsymbol{\theta}) / \partial \text{Im}\{h_k\} &= j \text{vec}[\mathbf{B}(k/W) \mathbf{A}^H(\boldsymbol{\theta}) - \mathbf{A}(\boldsymbol{\theta}) \mathbf{B}^H(k/W)] \end{aligned}$$

for $k = 0, \dots, L-1$.

As stated in [Zen97a, Theorem 2], the channel is identifiable if the channel Z-transform $H(z) \triangleq \sum_{k=0}^{L-1} h_k z^{-k}$ can be decomposed into N_{ss} subchannels having different reciprocal zeros⁴. When this condition is not hold, \mathbf{D}_r is singular for this channel realization (see Section 4.3). Notice that this condition is weaker than the usual identifiability condition [Ton95][Tug95].

6.4.2 Numerical Results

The simulated channel spreads over $N = 3$ symbol periods. The transmitted pulse $p(t)$ is a squared-root raised cosine of roll-off r truncated to last 8 symbols. The channel taps h_k are

⁴ z_0 is a reciprocal zero of $\mathcal{H}(z)$ if $\mathcal{H}(z_0) = \mathcal{H}(z_0^{-1}) = 0$.

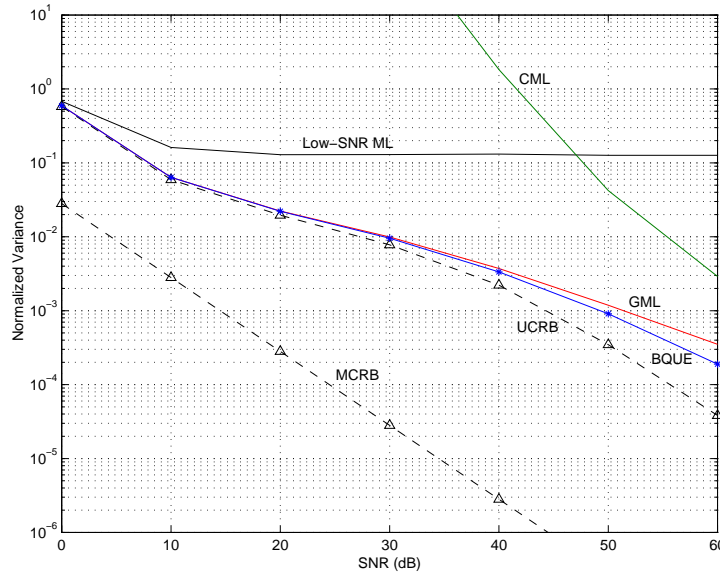


Figure 6.21: Performance of the second-order ML-based estimators (Low-SNR approximation, Conditional ML and Gaussian ML) and the optimal solution provided in Chapter 4. The simulation parameters are $r = 0.35$, $\mu = 0.02$ ($B_n = 5 \cdot 10^{-3}$).

generated as independent zero-mean Gaussian variables of unit variance. The receiver bandwidth is set to $W = 2/T$ to encompass any roll-off factor. Consequently, the number of taps is $L = NWT = 6$. The observation window is set to $M = 18$ samples and the received signal is oversampled taking $N_{ss} = 3$ samples per symbol. Finally, the transmitted symbols are QPSK.

The figure of merit computed in this section is the *normalized* variance of the estimator $\hat{\alpha}$ in the steady-state. The expected value with respect to the random channel will be computed in order to obtain the average performance of the estimator. Thus, the channel estimator variance is defined in the following way:

$$VAR \triangleq E_{\theta} \left\{ \frac{E \|\hat{\alpha}(n) - \alpha\|^2}{\|\alpha\|^2} \right\}$$

where the expectation with respect to θ is approximated by averaging 100 random channels.

The above figure of merit will be plotted as a function of the signal-to-noise ratio. The noise variance σ_w^2 will be adjusted at each realization to maintain the SNR since the received power depends on the actual channel response.

The ML-based estimators discussed in Chapter 3 and the corresponding bounds are evaluated and compared with the optimal second order estimator formulated in Chapter 4. In all the cases, a closed-loop scheme is implemented with its bandwidth adjusted to guarantee the *small-error*

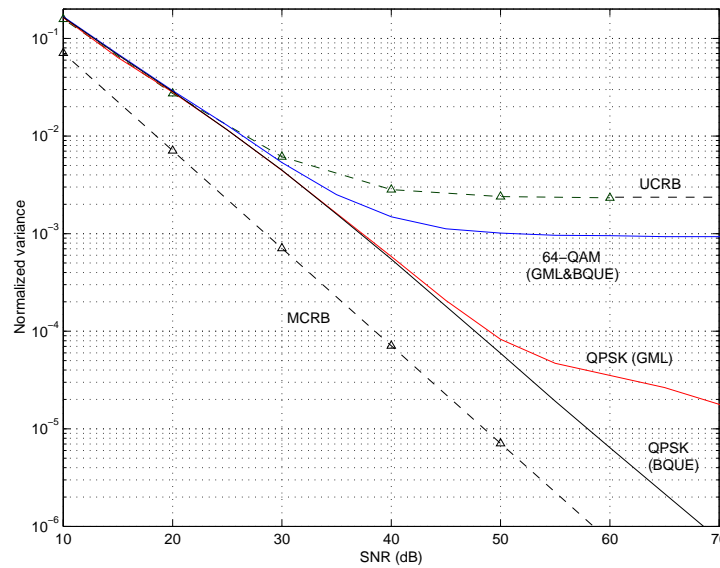


Figure 6.22: Comparison of the BQUE and GML estimators when the channel amplitude is estimated too and the transmitted symbols are QPSK, 64-QAM or, Gaussian distributed for a roll-off factor equal to 1.

condition for the simulated SNR range.

Suboptimal Algorithms comparison: Low-SNR ML, CML, GML

Using the CML method the channel can be determined up to a constant complex factor [Car00]. For comparison, all the methods will assume that the value of the first coefficient is 1.

Fig. 6.21 points out that the low-SNR approximation suffers from a severe high-SNR floor due to the self-noise contribution. On the other hand, the CML criterion is shown to be not useful for channel estimation because its variance is extremely high within the range of operative SNRs. Contrarily, the Gaussian model is shown to be appropriate to build good estimators of the channel response. Uniquely at high SNR, the exploitation of the discrete distribution of the symbols is found to improve the estimator accuracy.

The UCRB is also depicted showing that is a valid lower bound for the performance of second-order techniques. Nonetheless, in Fig. 6.21 the UCRB is shown to be a little optimistic in high-SNR scenarios. Finally, the MCRB predicts the theoretical performance that data-aided schemes would attain compared with second-order blind estimators. Clearly, the insertion of pilot symbols improves notably the estimator performance for any SNR. Additionally, another important advantage of DA methods is that they do not exhibit outliers at low SNR because

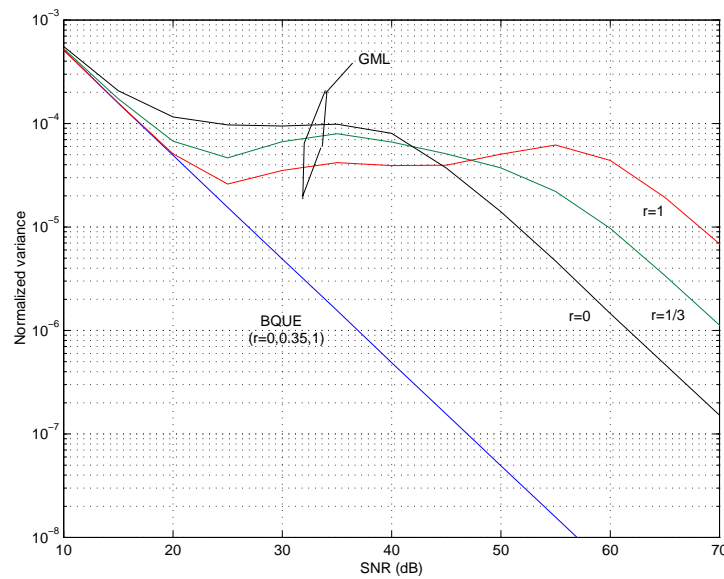


Figure 6.23: Comparison of the BQUE and GML estimators if the channel is multiplicative using different values of the roll-off factor.

the estimator is a linear transformation of the parameters.

Channel amplitude estimation: GML vs BQUE

In Fig. 6.22, the amplitude of the first channel tap is estimated too. The estimator variance exhibits a severe floor at high-SNRs due to the self-noise unless the symbols are drawn from a constant modulus constellation such as M-PSK or CPM. The floor level is inversely proportional to the observation time, which means that the estimator is consistent for any SNR, and is related to the amplitude dispersion of the constellation.

In order to clarify these conclusions, in Appendix 6.B the high-SNR asymptotic variances at high SNR for the GML and the optimal quadratic estimator is deduced when the transmitted signal is linearly modulated and the channel is multiplicative (Fig. 6.23). The asymptotic expressions obtained therein predict exactly the aforementioned floor showing its dependence on the constellation fourth-order moment ρ and the number of observed symbols.

Regarding the QPSK simulation ($\rho = 1$), the BQUE asymptotic variance is inversely proportional to the SNR whereas the GML performance degrades for high SNR (Fig. 6.22). The underlying motive is the poor estimation of the channel amplitude, as depicted in Fig. 6.23. In this figure, the GML suffers a *transitory* floor because the Gaussian assumption fails gradually as the SNR is augmented.

6.5 Angle-of-Arrival (AoA) Tracking

The classical approach in array signal processing considers that the sources are deterministic unknowns (conditional model) or, alternatively, *Gaussian* random variables (unconditional model) [Sto90a][Ott93]. As a consequence of the Central Limit Theorem, the Gaussian assumption provides optimal second-order DOA trackers with independence of the actual distribution of the sources if the number of sensors is asymptotically large [Sto89] or the SNR asymptotically low, as studied in Chapter 7.

However, in the context of mobile communications, the array size is limited and the above asymptotic condition is unrealistic. In these scenarios, the consideration of the discrete distribution of the transmitted signals yields a significant improvement in terms of tracking variance when two or more sources transmit from a similar DOA, even if the SNR is moderate. Notice that this improvement is not obtained exploiting the signal cyclostationarity [Gar88b][Sch89][Xu92][Rib96] because we consider that all the users transmit using the same modulation and, thus, share the same cyclostationarity. Nonetheless, it would be straightforward to incorporate this information if the received signal were oversampled as indicated in Section 6.1.

From this background, in the next subsection, we have sketched the formulation of the optimal second-order DOA tracker when the transmitted signals are digitally modulated. The performance of the resulting estimator constitutes the lower bound for the variance of any sample covariance based DOA estimator including the ML [Sto90a][Ott93] and subspace based methods such as the Pisarenko's [Pis73], MUSIC [Sch79][Bie80][Sto89], ESPRIT [Roy89], MODE [Sto90b], weighted subspace fitting (WSF) [Vib91] and other variants (see [Kri96][Ott93] and references therein). Notice that all these quadratic methods achieve the same asymptotic performance under appropriate hypothesis on the array manifold, when the observation time goes to infinity, as proved in [Ott92][Car94]. However, in this section they are shown to be inefficient –even in the asymptotic case– if the symbols are drawn from a constant modulus alphabet (e.g., MPSK or CPM).

The results in this section were presented in the IEEE Asilomar Conference on Signals, Systems and Computers that was held in Pacific Grove (USA) in 2003 [Vil03b]:

- “Second-Order DOA Estimation from Digitally Modulated Signals”, J. Villares, G. Vázquez, Proc. of the *37th IEEE Asilomar Conference on Signals, Systems and Computers*, Pacific Grove (USA), November 2003.

6.5.1 Signal Model

In all the estimation problems addressed in this chapter, the parameter $\boldsymbol{\theta}$ remains static during the observation time. However, in the context of mobile communications, it is important to obtain an accurate estimate of the users angular position but also to track their location as the transmitters move around the base station. Consequently, it is necessary to estimate both the angle and the angular speed of every source transmitting towards the base station. Higher-order derivatives of the AoA (acceleration and so on) will be disregarded from the study for simplicity. Therefore, based on the small-error estimators obtained in (4.12) and (4.18), a closed-loop scheme (tracker) as the one suggested in Section 2.5.2 will be implemented in order to track the parameter $\boldsymbol{\theta}_n$ evolution. To do so, the parameter dynamics (speed, acceleration, etc.) must be incorporated into the model.

Formally, let us consider the problem of tracking the angle-of-arrival of P narrowband sources impinging into a uniform linear array composed of M antennas spaced $\lambda/2$ meters, with λ the common signal wavelength. Let us consider that all the transmitters are visible from the base station array and they do not experience multipath propagation. Let $\boldsymbol{\phi}(t) \in [-\pi, \pi]^P$ be the temporal evolution of the P angles-of-arrival in radians and $\boldsymbol{\phi}'(t) \triangleq \partial\boldsymbol{\phi}(t)/\partial t$ the respective derivatives accounting for the angular speed. Let us assume that the acceleration and higher-order derivatives are negligible during the observation time, that is, $\partial^i\boldsymbol{\phi}(t)/\partial t^i = \mathbf{0}$ for $i > 1$. Furthermore, let us assume that the bandwidth of $\boldsymbol{\phi}(t)$ does not exceed $1/2T$, with T the symbol period. In that case, $\boldsymbol{\phi}(nT)$ holds the sampling theorem and the P trajectories can be ideally reconstructed from their samples $\boldsymbol{\phi}_n \triangleq \boldsymbol{\phi}(nT)$ yielding the following discrete-time dynamical model or state equation:

$$\boldsymbol{\phi}_{n-k} = \boldsymbol{\phi}_n - k\boldsymbol{\phi}'_n \quad (6.48)$$

where the angular speed $\boldsymbol{\phi}'_n$ is normalized to the symbol period T . Therefore, the composed vector of parameters that must be estimated to track the users without having any systematic pursuit error is

$$\boldsymbol{\theta}_{n+1} \triangleq \begin{bmatrix} \boldsymbol{\phi}_{n+1} \\ \boldsymbol{\phi}'_{n+1} \end{bmatrix} = \mathbf{G}\boldsymbol{\theta}_n \quad (6.49)$$

with

$$\mathbf{G} \triangleq \begin{bmatrix} \mathbf{I}_P & \mathbf{I}_P \\ \mathbf{0}_P & \mathbf{I}_P \end{bmatrix}$$

Consequently, the optimal second-order AoA tracker is given by

$$\widehat{\boldsymbol{\theta}}_{n+1} = \mathbf{G}\widehat{\boldsymbol{\theta}}_n + \text{diag}(\boldsymbol{\mu}) \mathbf{G}\mathbf{J}_2^\#(\widehat{\boldsymbol{\theta}}_n)\mathbf{D}_r^H \mathbf{Q}^{-1}(\widehat{\boldsymbol{\theta}}_n) \left(\widehat{\mathbf{r}} - \mathbf{r}(\widehat{\boldsymbol{\theta}}_n) \right), \quad (6.50)$$

using the small-error expression obtained in (4.12) with $\mathbf{D}_g = \mathbf{G}$. Notice that the above expression follows the structure of the optimal ML tracker in Section 2.5.2 with $\mathbf{h}(\boldsymbol{\theta}_n) = \mathbf{G}\boldsymbol{\theta}_n$.

The above solution forces to zero all the cross-derivatives of $\mathbf{g}(\boldsymbol{\theta})$ including the IPI terms associated to the interference from other users (Section 4.4). This interference is referred to as multiuser or multiple access interference (MUI or MAI) in the literature. Thus, the second-order AoA tracker in (6.50) will be referred to as the *MUI-free* AoA tracker hereafter.

On the other hand, following the reasoning in Section 4.4, it is not strictly necessary to cancel out the cross-derivatives corresponding to different users because the tracker optimization will remove the MUI contribution if the SNR is sufficiently high. Likewise, if the SNR is low, the MUI term will be automatically ignored to not enhance the noise contribution. Thus, it is only necessary to decouple the estimates of ϕ_n and ϕ'_n in order to have unbiased estimates of $\boldsymbol{\theta}_{n+1}$ in (6.49). If not, AoA estimation errors would yield angular speed deviations and vice versa. To avoid this, we have to constrain these cross-derivatives to zero, as indicated next:

$$\left. \frac{\partial [\widehat{\phi}_n]_p}{\partial [\phi'_n]_p} \right|_{\boldsymbol{\theta}=\widehat{\boldsymbol{\theta}}_n} = \left. \frac{\partial [\widehat{\phi}'_n]_p}{\partial [\phi_n]_p} \right|_{\boldsymbol{\theta}=\widehat{\boldsymbol{\theta}}_n} = 0 \quad p = 1, \dots, P \quad (6.51)$$

while the rest of cross-derivatives is liberated. We will refer to this solution as the *MUI-resistant* AoA tracker in the sequel.

To complete the signal model, the received signal is passed through the matched-filter and then sampled at one sample per symbol in order to collect K snapshots⁵. Independent snapshots are obtained assuming that the actual modulation is ISI-free and, consequently, the symbol synchronization has been established. On the other hand, it can be shown that carrier synchronization is not required since the matrix $\mathbf{Q}(\boldsymbol{\theta})$ is insensitive to the phase of the $P \times K$ nuisance parameters.

According to the considerations above, the snapshot recorded at time $n - k$ is given by

$$\mathbf{y}_{n-k} = \mathbf{A}_{n-k}(\boldsymbol{\theta}_n) \mathbf{x}_{n-k} + \mathbf{w}_{n-k}$$

where \mathbf{x}_{n-k} is the vector containing the symbols transmitted by the P users at time $n - k$, \mathbf{w}_{n-k} the *white* noise samples and the p -th column of $\mathbf{A}_{n-k}(\boldsymbol{\theta}_n)$,

$$[\mathbf{A}_{n-k}(\boldsymbol{\theta}_n)]_p \triangleq \begin{bmatrix} 1 \\ \exp \left[j\pi \sin \left([\phi_n]_p - k [\phi'_n]_p \right) \right] \\ \vdots \\ \exp \left[j\pi (M-1) \sin \left([\phi_n]_p - k [\phi'_n]_p \right) \right] \end{bmatrix},$$

⁵Notice that the problem dynamics (angle and angular velocity) require to process $K \geq 2$ snapshots.

is the steering vector associated to the p -th source at time $n - k$ with $j \triangleq \sqrt{-1}$. Notice that $\mathbf{A}_{n-k}(\boldsymbol{\theta}_n)$ incorporates the known dynamical model (6.48).

In order to reproduce the vectorial model in (2.13), the K snapshots are stacked to build the following spatio-temporal observation:

$$\mathbf{y}(n) \triangleq \begin{bmatrix} \mathbf{y}_n \\ \vdots \\ \mathbf{y}_{n-K+1} \end{bmatrix} = \mathbf{A}(\boldsymbol{\theta}_n) \mathbf{x}(n) + \mathbf{w}(n)$$

where $\mathbf{x}(n)$ and $\mathbf{w}(n)$ are constructed as $\mathbf{y}(n)$ and the transfer matrix $\mathbf{A}(\boldsymbol{\theta}_n)$ is given by

$$\mathbf{A}(\boldsymbol{\theta}_n) \triangleq \begin{bmatrix} \mathbf{A}_n(\boldsymbol{\theta}_n) & & \\ & \ddots & \\ & & \mathbf{A}_{n-K+1}(\boldsymbol{\theta}_n) \end{bmatrix}$$

As stated before, once the signal model has been determined, we only have to find the set of constituent matrices in (4.12) and (4.18). To conclude, the derivatives of the steering vectors are provided next:

$$\begin{aligned} \frac{\partial [\mathbf{A}_{n-k}(\boldsymbol{\theta}_n)]_{p,m}}{\partial [\phi_n]_q} &= j\pi m \cos([\phi_n]_p - k[\phi'_n]_p) \exp[j\pi \sin([\phi_n]_p - k[\phi'_n]_p)] \delta(p - q) \\ \frac{\partial [\mathbf{A}_{n-k}(\boldsymbol{\theta}_n)]_{p,m}}{\partial [\phi'_n]_q} &= -j\pi m k \cos([\phi_n]_p - k[\phi'_n]_p) \exp[j\pi \sin([\phi_n]_p - k[\phi'_n]_p)] \delta(p - q) \end{aligned}$$

for all $p, q \in \{1, \dots, P\}$ where $\delta(\cdot)$ stands for the Kronecker delta.

6.5.2 Numerical Results

Two independent sources transmitting from the far-field to a uniform linear array composed of $M = 4$ antennas are simulated. The received power is assumed to be the same for simplicity. Both signals are QPSK modulated and two snapshots ($K = 2$) are recorded at the matched-filter output.

The figure of merit considered in this section is the estimator normalized steady-state variance defined as

$$\text{VAR}(\Delta\phi) \triangleq \frac{E \left\| \hat{\phi}_n - \phi_n \right\|^2}{P\Delta\phi^2} \quad (6.52)$$

with $\Delta\phi \triangleq ([\phi_n]_2 - [\phi_n]_1)/2$ half of the sources separation. The variance will be plotted as a function of the SNR *per source* at the matched-filter output $E_s/N_0 = \sigma_w^{-2}$ with E_s the received symbol energy and N_0 the noise double-sided spectral density.

Two AoA trackers forcing a different set of constraints on $\mathbf{g}(\boldsymbol{\theta})$ will be tested:

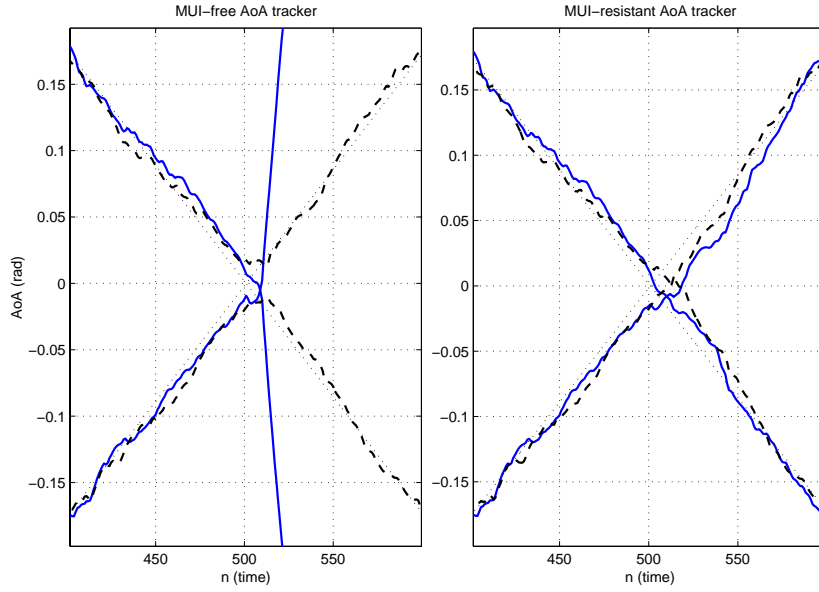


Figure 6.24: AoA tracking of two users whose trajectories cross at time instant $n=500$. The output of the MUI-free and MUI-resistant trackers is plotted on the left and right hand side, respectively. Two simulations are run with two different outcomes for the MUI-free tracker: tracking is lost (solid line) or the two sources are interchanged (dashed line). The signal SNR is fixed to 10 dB in both cases.

1. *MUI-free AoA tracker*: $\mathbf{M}^H \mathbf{D}_r = \mathbf{D}_g = \mathbf{I}_P$;
2. *MUI-resistant AoA tracker*: $\text{diag}(\mathbf{M}^H \mathbf{D}_r) = \text{diag}(\mathbf{D}_g) = \text{diag}(\mathbf{I}_P)$ and the cross terms in (6.51) are set to zero.

Two different scenarios have been simulated in order to illustrate the benefit of considering the actual distribution of the sources when they are transmitting from similar angles.

Two users crossing

Figure 6.24 shows that the MUI-free AoA tracker (left plot) loses tracking as the two sources approach each other due to the noise enhancement observed when the SNR is low (SNR=10dB). This situation arises because, when the users are transmitting from similar angles, the matrix \mathbf{D}_r becomes nearly singular and the estimator variance (4.13) augments suddenly.

On the other hand, the MUI-resistant AoA tracker (right plot) overcomes this critical situation because it does not try to remove the MUI term associated to the cross derivatives of \mathbf{D}_r when the noise contribution is dominant (low SNR). Following the explanation in Section 4.4,

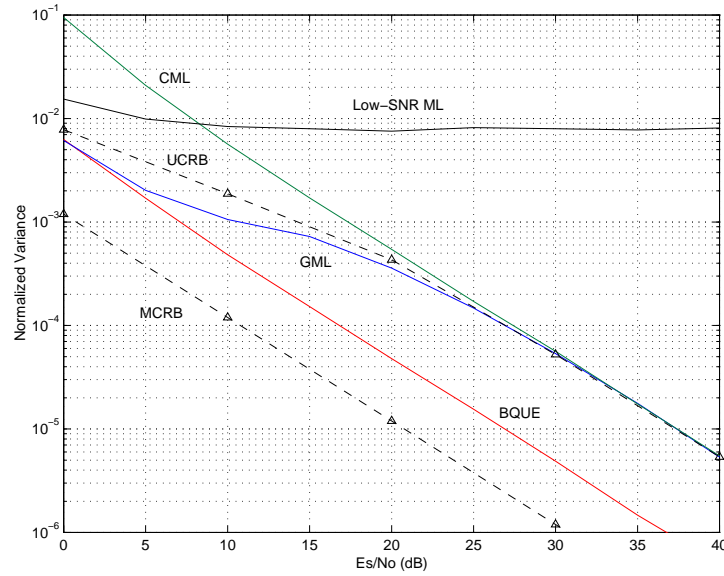


Figure 6.25: Steady-state variance of the AoA tracker for two sources located at ± 5 degrees from the broadside. The loop-bandwidth is set to $B_n = 1.25 \cdot 10^{-3}$ and the MUI-free estimator is simulated.

the MUI-resistant AoA tracker liberates the cross derivatives in \mathbf{D}_r while the users are crossing and matrix \mathbf{D}_r is badly conditioned. In this manner, the tracker does not enhance the noise contribution and is able to remain “locked” during the crossing.

Steady-state variance for two near sources

The steady-state variance of the MUI-free AoA tracker is evaluated as a function of the SNR, considering that we have two still users separated 10° (Fig. 6.25) and 1° (Fig. 6.26). The noise equivalent loop bandwidth B_n (Section 2.5.2) has been selected in order to guarantee the small-error condition for all the simulated SNRs (Section 4). For the studied set-up, the noise enhancement caused by the sources proximity is found to be negligible. This fact makes the two suggested implementations (MUI-resistant and MUI-free) to be practically equivalent in the simulated scenarios. A minor improvement is appreciated in Fig. 6.26 for low SNR.

Theoretically, the performance of the MUI-free estimator is very limited at low SNR when the two sources are close, as shown in figure 6.27, whereas its competitor (MUI-resistant) achieves the single user performance whatever the simulated SNR. Thus, Fig. 6.27 illustrates the potential gain that the MUI-resistant alternative offers in terms of steady-state variance when the problem is badly conditioned and the observations are very corrupted by the noise.

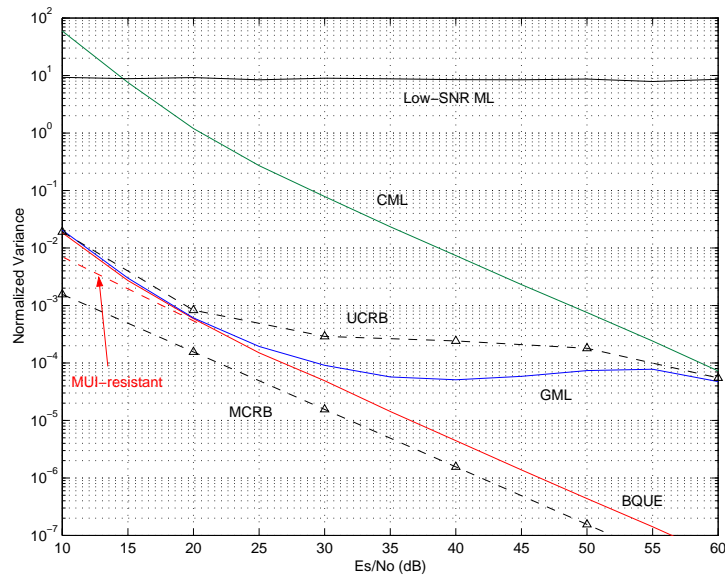


Figure 6.26: Steady-state variance of the AoA tracker for two sources located at ± 0.5 degrees from the broadside. The loop-bandwidth is set to $B_n = 1.65 \cdot 10^{-4}$ and the MUI-free estimator is simulated.

In Fig. 6.25 and Fig. 6.26, the optimal second-order tracker has also been compared with the ML-based trackers formulated in Section 2.4. The first conclusion is that the low-SNR approximation appears to be useless in these critical scenarios for the SNRs of interest. The underlying motive is the so-called self-noise, i.e., the variance floor caused by the nuisance parameters at high SNR (Section 2.4.1). The self-noise is really irrelevant when the SNR tends to zero but it becomes dominant as soon as the SNR is increased. Notice that, in the AoA estimation problem at hand, the so-called *self-noise* is generated by the random symbols (nuisance parameters) from the user of interest as well as the other interfering users. Therefore, the MUI and self-noise contributions are strongly connected in this case study.

To overcome the low-SNR UML variance floor, the CML tracker was proposed in Section 2.4.2. The CML is able to yield self-noise free estimates but it suffers from noise enhancement when the SNR is low because it tries to decorrelate the nuisance parameters from the different users.

Regarding the GML AoA tracker presented in Section 2.4.3, the convergence to the CML solution for high SNR and to the low-SNR UML solution for low SNR (if the x -axis were expanded) is observed. Between these two asymptotic extremes, the GML adjusts its coefficients depending on the actual SNR to minimize the joint contribution of the noise and the self-noise. Indeed, the GML solution is found to be the best quadratic estimator or tracker based uniquely

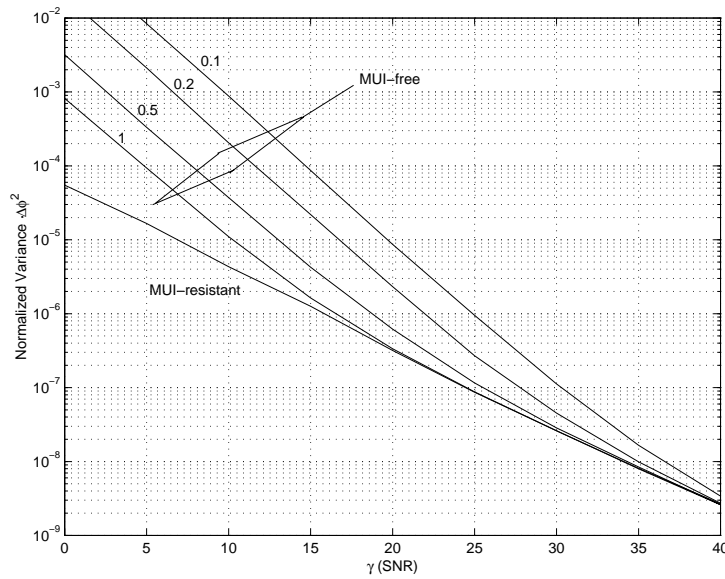


Figure 6.27: Normalized variance as a function of the SNR for the MUI-free and MUI-resistant AoA trackers when the sources are separated 0.1, 0.2, 0.5 or 1 as indicated for each curve. The tracker loop bandwidth is set to $B_n = 1.25 \cdot 10^{-3}$.

on the second-order moments of the nuisance parameters, i.e., if $\mathbf{K} = \mathbf{0}$ in (3.10). Nonetheless, when comparing the variance of the GML and the BQUE AoA trackers in Figs. 6.25-6.26, it is confirmed that second-order estimation is improved for medium-to-high SNRs if the fourth-order statistical knowledge on the nuisance parameters ($\mathbf{K} \neq \mathbf{0}$) is exploited. The resulting gain is shown to be greater when the angular separation is reduced if one compares Fig. 6.25 and Fig. 6.26. Moreover, when the loop bandwidth B_n is small (Fig. 6.26), the BQUE performance is rather close to the one predicted by the MCRB in case of known nuisance parameters and, it definitely constitutes the lower bound for the variance of any unbiased estimator based on the sample covariance matrix.

Surprisingly, the GML estimator does not attain the UCRB bound out of the aforementioned asymptotic cases because the nuisance parameters are actually non-Gaussian (QPSK discrete symbols) and the UCRB is based on the Gaussian assumption.

Appendix 6.A Computation of \mathbf{Q} for carrier phase estimation

The expected value of $\nabla^2(\mathbf{y}; \theta_o)$ (6.12) can be manipulated as follows

$$\begin{aligned} E\{\nabla^2(\mathbf{y}; \theta_o)\} &= 4\sigma_w^{-8} E\left\{\text{Im}^2\left\{e^{-j2\theta_o} \mathbf{r}^H \tilde{\mathbf{r}}\right\}\right\} = -\sigma_w^{-8} E\left\{\left(e^{-j2\theta_o} \mathbf{r}^H \tilde{\mathbf{r}} - e^{j2\theta_o} \tilde{\mathbf{r}}^H \mathbf{r}\right)^2\right\} \\ &= 2\sigma_w^{-8} \left(\mathbf{r}^H E\{\tilde{\mathbf{r}}\tilde{\mathbf{r}}^H\} \mathbf{r} - \text{Re}\left(e^{-j4\theta_o} \mathbf{r}^H E\{\tilde{\mathbf{r}}\tilde{\mathbf{r}}^T\} \mathbf{r}^*\right)\right) \\ &= 2\sigma_w^{-8} \mathbf{r}^H \left(E\{\tilde{\mathbf{r}}\tilde{\mathbf{r}}^H\} - e^{-j4\theta_o} E\{\tilde{\mathbf{r}}\tilde{\mathbf{r}}^T\}\right) \mathbf{r} \end{aligned}$$

bearing in mind that both Γ and $E_{\mathbf{x}}\{\text{vec}(\mathbf{xx}^T) \text{vec}^T(\mathbf{xx}^T)\}$ are real amounts for any CPM signal according to the Laurent's expansion [Lau86]. In that case, the proper and improper correlation matrices of $\tilde{\mathbf{r}}$ can be computed as follow:

$$\begin{aligned} E\{\tilde{\mathbf{r}}\tilde{\mathbf{r}}^T\} &= e^{j4\theta_o} \mathcal{A} E_{\mathbf{x}}\{\text{vec}(\mathbf{xx}^T) \text{vec}^T(\mathbf{xx}^T)\} \mathcal{A}^T \\ E\{\tilde{\mathbf{r}}\tilde{\mathbf{r}}^H\} &= \mathcal{A} E_{\mathbf{x}}\{\text{vec}(\mathbf{xx}^T) \text{vec}^H(\mathbf{xx}^T)\} \mathcal{A}^H + \\ &\quad + (\mathbf{I} + \mathcal{K})(\mathbf{R}_w \otimes \mathbf{A}\mathbf{A}^H) + (\mathbf{I} + \mathcal{K})(\mathbf{A}\mathbf{A}^H \otimes \mathbf{R}_w) + \\ &\quad + (\mathbf{I} + \mathcal{K})(\mathbf{R}_w \otimes \mathbf{R}_w) \\ &= \mathcal{A} [E_{\mathbf{x}}\{\text{vec}(\mathbf{xx}^T) \text{vec}^H(\mathbf{xx}^T)\} - 2\mathcal{P}] \mathcal{A}^H + 2\mathcal{P} (\bar{\mathbf{R}} \otimes \bar{\mathbf{R}}) \end{aligned}$$

where $\mathcal{P} \triangleq \frac{1}{2}(\mathbf{I} + \mathcal{K})$ and the following identities have been applied as done in Appendix 3.B:

$$\begin{aligned} \text{vec}(\mathbf{ABC}^T) &= (\mathbf{C} \otimes \mathbf{A}) \text{vec}(\mathbf{B}) \\ (\mathbf{A} \otimes \mathbf{B})(\mathbf{C} \otimes \mathbf{D}) &= \mathbf{AC} \otimes \mathbf{BD} \\ \text{vec}(\mathbf{ab}^T) \text{vec}^H(\mathbf{ab}^T) &= (\mathbf{b} \otimes \mathbf{a})(\mathbf{b} \otimes \mathbf{a})^H = \mathbf{bb}^H \otimes \mathbf{aa}^H \\ \text{vec}(\mathbf{ba}^T) \text{vec}^H(\mathbf{ab}^T) &= \mathcal{K} \text{vec}(\mathbf{ab}^T) \text{vec}^H(\mathbf{ab}^T) = \mathcal{K}(\mathbf{bb}^H \otimes \mathbf{aa}^H) = (\mathbf{aa}^H \otimes \mathbf{bb}^H) \mathcal{K}. \end{aligned}$$

Finally, if \mathbf{Q} is defined as

$$\mathbf{Q} \triangleq \mathcal{A}\mathbf{K}\mathcal{A}^H + 2\bar{\mathbf{R}} \otimes \bar{\mathbf{R}}$$

with \mathbf{K} given in (6.19), then

$$E\{\nabla^2(\mathbf{y}; \theta_o)\} = 2\sigma_w^{-8} \mathbf{r}^H \mathcal{P} \mathbf{Q} \mathbf{r} = 2\sigma_w^{-8} \mathbf{r}^H \mathbf{Q} \mathbf{r}$$

using the following properties of the orthogonal projector \mathcal{P} :

$$\begin{aligned} \mathcal{P}\mathcal{A}\mathbf{K}\mathcal{A}^T &= \mathcal{A}\mathcal{P}\mathbf{K}\mathcal{A}^T = \mathcal{A}\mathbf{K}\mathcal{A}^T \\ \mathcal{P}\mathbf{r} &= \mathbf{r}. \end{aligned}$$

Appendix 6.B Asymptotic expressions for multiplicative channels

Let $\mathbf{y} = a\mathbf{x} + \mathbf{w}$ be the matched filter output with $a \in (0, +\infty)$ the amplitude we aim to estimate, \mathbf{x} the vector of N symbols and \mathbf{w} the AGW noise of variance σ_w^2 . From this simple model and after some manipulations, the variance of the GML and BQUE estimators is identical and is given by

$$VAR = B_{UCRB} + \frac{a^2(\rho - 2)}{4N}$$

where B_{UCRB} denotes the associated UCRB (Section 2.6.1):

$$B_{UCRB} = \frac{(a^2 + \sigma_w^2)^2}{4Na^2}$$

If we take the limit of VAR when the noise variance tends to zero, we obtain

$$VAR = \frac{a^2(\rho - 1)}{4N} + \frac{\sigma_w^2}{2N} + o(\sigma_w^2),$$

that only goes to zero as the noise vanishes if $N \rightarrow \infty$ (consistent estimator) or $\rho = 1$, which is the case of the MPSK modulation, proving that the signal amplitude can only be perfectly estimated from a finite observation in case of constant amplitude modulations such as the MPSK.

Finally, notice that the performance of the GML and the BQUE is generally different if the estimator operates directly on the received signal as shown in Fig. 6.23.